LOCAL MASS-CORRECTIONS FOR CONTINUOUS PRESSURE APPROXIMATIONS OF INCOMPRESSIBLE FLOW

B. GMEINER , C. WALUGA*, AND B. WOHLMUTH

Abstract. In this work, we discuss a family of finite element discretizations for the incompressible Stokes problem using continuous pressure approximations on simplicial meshes. We show that after a simple and cheap correction, the mass-fluxes obtained by the considered schemes preserve local conservation on dual cells without reducing the convergence order. This allows the direct coupling to vertex-centered finite volume discretizations of transport equations. Further, we can postprocess the mass fluxes independently for each dual box to obtain an element-wise conservative velocity approximation of optimal order that can be used in cell-centered finite volume or discontinuous Galerkin schemes. Numerical examples for stable and stabilized methods are given to support our theoretical findings. Moreover, we demonstrate the coupling to vertex- and cell-centered finite volume methods for advective transport.

Key words. Stokes equations, mixed finite elements, stabilization, local mass conservation.

AMS subject classifications. 76D05, 76D07, 65F10, 65N30

1. Introduction.

In this work, we consider the iso-viscous Stokes problem

$$-\Delta \mathbf{u} + \nabla p = \mathbf{f}, \qquad \text{in } \Omega, \tag{1.1a}$$

$$\operatorname{div} \mathbf{u} = 0, \qquad \text{in } \Omega, \tag{1.1b}$$

as a prototype for incompressible flow in an open bounded domain $\Omega \subset \mathbb{R}^d$, $d = 2, 3$. Here, $\mathbf{u} = [u_1, \dots, u_d]^\top$ denotes the velocity field, p the pressure, and $\mathbf{f} = [f_1, \dots, f_d]^\top$ stands for a forcing term. Below we agree on the convention, that all vectorial quantities are printed in bold. For simplicity, we consider homogeneous Dirichlet boundary conditions, i.e., we set $\mathbf{u} = \mathbf{0}$ on $\partial\Omega$, and to make the pressure well-defined, we further set $\int_\Omega p \, \mathrm{d}x = 0$. More general boundary conditions are considered in our numerical tests. These may be incorporated by the usual techniques; cf. [39] for an overview.

The Stokes problem written in the form of (1.1) is well-studied in the mathematical literature, and there exist a number of widely-used discretization schemes. A common problem which is faced here is a compatibility condition on the discrete spaces in which the velocity and pressure are interpolated, the so-called LBB condition named after Ladyzhenskaya, Babuška and Brezzi. A seemingly natural placement of the degrees of freedom is employed in staggered discretizations, e.g., the MAC scheme [30]. Such staggered schemes often result in lightweight stencils that preserve desirable physical properties like local mass-conservation which may be important when we want to avoid spurious sources and sinks if the computed flow field is employed for transporting physical quantities [14, 18]. However, these methods often have the drawback that they are not easily generalizable to unstructured meshes and/or higher orders. While finite element discretizations are usually geometrically more flexible, the most-appealing choices are known to be notoriously unstable [10, 7]. For example, it is well-known that equal-order conforming interpolations produce spurious pressure modes and violate the physical principle of local mass-conservation. The former problem can be controlled by adding stabilization terms on the discrete level. The latter

*Institute for Numerical Mathematics (M2), Technische Universität München, Boltzmannstrasse 3, D–85748 Garching b. München, Germany; Corresponding author: waluga@ma.tum.de

problem is often addressed in the literature by either penalizing the divergence of the discrete velocity field (grad-div-stabilization; cf. [38, 13]) or by enlarging the velocity space, thereby allowing piecewise discontinuous pressure approximations, which in turn allow for enhanced local mass-conservation. Among the most popular methods of this class are higher-order conforming finite elements [17, 11], and nonconforming schemes, such as the Crouzeix–Raviart element [17] or the rapidly developing class of discontinuous Galerkin methods [44, 25, 40, 16, 15, 20]. However, while some of these schemes can be efficiently implemented on modern architectures, they are expensive in terms of degrees of freedom per accuracy, and they impose a considerable infrastructural demand on the underlying framework. In particular, if the required data-structures are not or incompletely implemented in a given framework, it is practically impossible to realize any of these methods efficiently without making massive extensions to the underlying codebase first. The situation gets even worse when we consider implementations involving highly optimized communication structures for parallel processing on extreme scales; cf., e.g., the discussion in [26]. It is partly because of the facts listed above, that nowadays, still many successful academic and commercial computational fluid dynamics codes are based on a specific choice of finite differences, finite volumes or continuous finite elements of low order, such as stabilized equal-order elements or the second order Taylor–Hood elements.

In this work, we aim to overcome the commonly criticized lack of local mass conservation for a large class of continuous-pressure finite element discretizations, which we describe in detail in Section 2. We do this by introducing a unified but abstract mass flux correction for this type of methods in Section 3, which is defined on the faces of a dual mesh. We then discuss a postprocessing procedure which allows the lifting of the mass fluxes to obtain a pointwise solenoidal velocity approximation, and we prove that the postprocessing does not deteriorate the order of convergence of the original solution. Section 4 is devoted to the concrete construction of conservative mass-fluxes for some examples of stabilized finite element methods based on linear equal-order pairings. Our theoretic considerations are complemented by numerical examples in Section 5. Here we particularly point out the importance of exact local mass conservation in coupled simulations of flow and transport.

2. Finite element discretization. Suppose a given polyhedral domain $\Omega \subset \mathbb{R}^d$ which is subdivided into simplices to obtain a quasi-uniform triangulation $\mathcal{T}_h$ satisfying the usual shape-regularity assumptions. For $k_V \geq k_Q \geq 1$, we define the velocity and pressure spaces by

$$\begin{aligned}\mathbf{V}_h &:= \{\mathbf{v}_h \in [H_0^1(\Omega)]^d : \mathbf{v}_h|_T \in [P_{k_V}(T)]^d,\ \forall T \in \mathcal{T}_{h_V}\},\\ Q_h &:= \{q_h \in H^1(\Omega) : q_h|_T \in P_{k_Q}(T),\ \forall T \in \mathcal{T}_{h_Q}\}.\end{aligned}$$

It is well-known that the natural choice $k_V = k_Q = 1$ and $h_V = h$, $h_Q = h$ does not give a uniformly stable pairing [11]. This observation motivates us to consider also velocity spaces on a finer mesh. In the case that $h_V \neq h$, we assume that $\mathcal{T}_{h/2}$ is obtained by uniform refinement from $\mathcal{T}_h$ and set $h_V = h/2$. An example for such a choice is $h_V = h/2$, $h_Q = h$ and $k_V = 1 = k_Q$, i.e., the stable modified Taylor–Hood element, also called P_1-iso-$P_2 - P_1$. Setting $k_V = 1 = k_Q$ and $h_V = h/2 = h_Q$, we obtain an unstable pairing which can be stabilized in terms of a two-level stabilization, see, e.g., [41] or Section 4.3. To formally incorporate the mean-value condition of the pressure, we further define $Q_h^0 := Q_h \cap L_0^2(\Omega)$.

We then consider the following weak formulation for discretizing the Stokes prob-

lem: find $(\mathbf{u}_h, p_h) \in \mathbf{V}_h \times Q_h^0$ such that

$$a(\mathbf{u}_h, \mathbf{v}_h) + b(\mathbf{v}_h, p_h) = f(\mathbf{v}_h), \qquad \mathbf{v}_h \in \mathbf{V}_h, \tag{2.1a}$$

$$b(\mathbf{u}_h, q_h) - c_h(p_h, q_h) = g_h(q_h), \qquad q_h \in Q_h, \tag{2.1b}$$

where we define the bilinear forms as

$$a(\mathbf{u}, \mathbf{v}) := \int_\Omega \nabla \mathbf{u} : \nabla \mathbf{v} \, \mathrm{d}x, \quad \text{and} \quad b(\mathbf{u}, q) := -\int_\Omega \operatorname{div} \mathbf{u} \cdot q \, \mathrm{d}x,$$

and the linear form as $f(\mathbf{v}) := \int_\Omega \mathbf{f} \cdot \mathbf{v} \, \mathrm{d}x$. The bilinear form $c_h(\cdot,\cdot) := \sum_{T \in \mathcal{T}_h} c_T(\cdot,\cdot)$ and the linear functional $g_h(\cdot) := \sum_{T \in \mathcal{T}_h} g_T(\cdot)$ may be required to stabilize the finite element pairing $\mathbf{V}_h \times Q_h$ if the following uniform LBB condition is violated:

$$\inf_{q_h \in Q_h^0} \sup_{\mathbf{v}_h \in \mathbf{V}_h} \frac{b(\mathbf{v}_h, q_h)}{a(\mathbf{v}_h, \mathbf{v}_h)^{1/2} \|q_h\|_0} \geq \beta,$$

for $\beta > 0$ independent of h. Moreover, we require discrete local continuity, semi-coercivity and symmetry of $c_h(\cdot,\cdot)$, discrete continuity of $g_h(\cdot)$ and the compatibility conditions $c_h(\cdot, 1) = 0$, $g_h(1) = 0$. To simplify notation, we introduce the bilinear form

$$S_h(\mathbf{u}, p; \mathbf{v}, q) := a(\mathbf{u}, \mathbf{v}) + b(\mathbf{v}, p) + b(\mathbf{u}, q) - c_h(p, q)$$

which allows us to write the discrete problem as: find $(\mathbf{u}_h, p_h) \in \mathbf{V}_h \times Q_h^0$ such that

$$S_h(\mathbf{u}_h, p_h; \mathbf{v}_h, q_h) = f(\mathbf{v}_h) + g_h(q_h), \qquad (\mathbf{v}_h, q_h) \in \mathbf{V}_h \times Q_h. \tag{2.2}$$

We recall that the choice of homogeneous Dirichlet boundary conditions automatically guarantees that the condition $\int_{\partial\Omega} \mathbf{u}_h \cdot \mathbf{n} \, \mathrm{d}s = 0$ holds. To establish existence, uniqueness and a priori results of discrete solutions, we hence assume that the discrete Stokes formulation (2.1) is uniformly stable, i.e., there exists a stability constant $\gamma > 0$ independent of h such that

$$\sup_{\mathbf{v}_h \in \mathbf{V}_h} \sup_{q_h \in Q_h^0} \frac{S_h(\mathbf{v}_h, q_h; \mathbf{w}_h, r_h)}{\|(\mathbf{v}_h, q_h)\|} \geq \gamma \|(\mathbf{w}_h, r_h)\|, \tag{2.3}$$

for all $\mathbf{w}_h \in \mathbf{V}_h$, and all $r_h \in Q_h^0$ with $\|(\mathbf{v}, q)\| := \left(\|\mathbf{v}\|_1^2 + \|q\|_0^2\right)^{1/2}$, $(\mathbf{v}, q) \in [H_0^1(\Omega)]^d \times L_0^2(\Omega)$. Given these stability results, the energy error can be bounded by a best-approximation error and the consistency error.

THEOREM 2.1. *Let $(\mathbf{u}, p)$ be the solution of the Stokes problem (1.1) and let $(\mathbf{u}_h, p_h) \in \mathbf{V}_h \times Q_h$ be the solution of the discrete problem (2.1). Moreover assume that the stability assumption (2.3) holds, then we get*

$$\|(\mathbf{u} - \mathbf{u}_h, p - p_h)\| \leq C \left(\inf_{\mathbf{v} \in V_h} \|(\mathbf{u} - \mathbf{v}, p - \Pi_h p)\| + \sup_{q \in Q_h} \frac{c_h(\Pi_h p, q) + g_h(q)}{\|q\|_0} \right),$$

where $\Pi_h p$ is the L^2-orthogonal projection of p onto Q_h.

Proof. The proof follows the lines of [7, Sect. 5.5.1] and is thus not repeated. ∎

The bilinear form $c_h(\cdot,\cdot)$ and the linear form $g_h(\cdot)$ have to satisfy a consistency condition to guarantee best approximation order a priori estimates. Let $k := \min(k_V, k_Q + 1)$ and assume that for $p \in H^k(\Omega)$

$$\sup_{q \in Q_h} \frac{c_h(\Pi_h p, q) + g_h(q)}{\|q\|_0} \leq C h^k |p|_k, \tag{2.4}$$

we then obtain in terms of Theorem 2.1 that $\|(\mathbf{u}-\mathbf{u}_h, p-p_h)\| = \mathcal{O}(h^k)$ provided that the solution is in $[H^{k+1}(\Omega)]^d \times H^k(\Omega)$. Furthermore under a suitable regularity assumption of the dual problem [28], the dual consistency assumption

$$\sup_{q\in Q_h} \frac{c_h(\Pi_h p, q) + g_h(q)}{\|q\|_1} \leq C h^{k+1} |p|_k, \tag{2.5}$$

and the dual continuity $|c_h(q_h, r_h)| \leq Ch\|q_h\|_0 |r_h|_1$, $r_h, q_h \in Q_h$, we get the estimate

$$h\|(\mathbf{u}-\mathbf{u}_h, p-p_h)\| + \|\mathbf{u}-\mathbf{u}_h\|_0 = \mathcal{O}(h^{k+1}), \tag{2.6}$$

by a duality argument of Aubin–Nitsche type [7, Sect. 5.5.5].

Before we close this section, some remarks are in order.

REMARK 2.2. *The results given in this work straightforwardly generalize to the case where $\mathbf{V}_h$ is enriched by some discrete function space $\mathbf{B}_h \subset [H_0^1(\Omega)]^d$. Typically $\mathbf{B}_h$ is associated with some higher order finite elements, e.g., the element-bubble functions of order $d+1$ of the MINI element [2].*

REMARK 2.3. *Under mild assumptions on the stabilization terms superconvergence results can be obtained for the choice $k_V = 1 = k_Q$ on a family on uniformly refined meshes. More precisely an order $\frac{1}{2}$ in the a priori bounds for the pressure can be recovered, see, e.g., [21]. This observation and the simplicity of the data-structures make this equal-order pairing particularly attractive for coupled large-scale simulations; cf. [26, 27] for recent work in this direction.*

3. Local mass conservation in an abstract setting. A common problem of continuous pressure finite element methods is that they do not preserve the physical concept of mass-conservation in a local sense. Namely, although the discrete solution $\mathbf{u}_h \in \mathbf{V}_h$ satisfies (2.1b), it is not element-wise mass conservative, i.e., since the pressure space does not include piecewise constants, we cannot, in general, expect

$$\int_{\partial T} \mathbf{u}_h \cdot \mathbf{n} \, \mathrm{d}s = 0, \quad T \in \mathcal{T}_{h_V},$$

to hold. Let us remark that this property alone does not necessarily yield small pointwise values of the divergence if $\operatorname{div} \mathbf{V}_h \neq Q_h$ or if stabilization terms enter the variational scheme. However it is a necessary condition to enable an element-by-element postprocessing to obtain strongly divergence-free velocities.

The lack of element-wise mass conservation in continuous pressure schemes has led many practitioners towards discontinuous pressure elements which are readily available at least in 2D for higher order velocity spaces. In 3D the situation is different, e.g., the choice $k_V = 2$ and a piecewise constant pressure space on the same mesh is uniformly stable in 2D but not in 3D, since here the second-order polynomials do not contain face-bubbles, see Figure 1. As a consequence, other popular choices such as the Taylor–Hood element enriched with piecewise constant pressures [22, Sect. 5.3.3] also require stabilization for the important case $d = 3, k_Q = 1$ [8]. For strongly divergence-free mixed finite elements, such as the Scott–Vogelius pair $P_k - P_{k-1}^{\mathrm{disc}}$, stability is only granted for $k \geq 3$ on macro-element type meshes [45] which complicates the implementation of solvers based on a hierarchic decomposition of the discrete function spaces, such as multilevel methods. On the other hand, adding bubble functions for stabilization of the Scott–Vogelius element destroys the strong mass conservation, and hence an additional postprocessing may be necessary; cf. e.g. [36] for details.

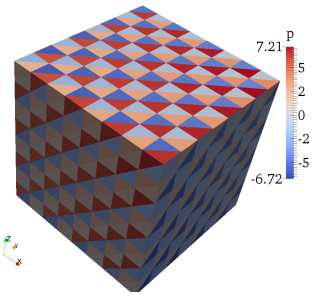

FIG. 1. *Example of a checkerboard instability in the pressure for a $P_2 - P_0$ pairing in 3D. The discrete solution was obtained on an $8 \times 8 \times 8$ structured tetrahedral mesh by solving* (2.1) *with homogeneous Dirichlet boundary conditions and* $\mathbf{f} = (1, 1, 1)^\top$.

In the following, we shall discuss the conservation properties of continuous pressure schemes for the class of discretization schemes outlined in the abstract setting above. Later we consider examples of stable or stabilized pairings of spaces proposed in the literature. In particular, we shall demonstrate that a local post-processing can recover the mass conservation on dual mesh cells, which in turn can be used for local equilibration also on the primal mesh elements. For the ease of presentation, we shall assume $h_V = h_Q$ unless mentioned otherwise. A class of methods where $h_V \neq h_Q$ will be discussed in detail in Section 4.3.

3.1. Preliminary considerations. To start with, we associate with any conforming triangulation $\mathcal{T}_h$ a barycentric dual grid $\mathcal{B}_h$. The dual boxes are linked to the vertices $\mathbf{p} \in \mathcal{P}_h$ of the original mesh $\mathcal{T}_h$. In the 2D setting, we proceed as follows: Let $\mathbf{p} \in \mathcal{P}_h$ and denote by $\mathcal{E}_p$ the edges sharing the node $\mathbf{p}$. Then, if $e \in \mathcal{E}_p$ is a boundary edge, we connect the midpoint $\mathbf{b}_e$ of e with $\mathbf{p}$ and to the barycenter $\mathbf{b}_T$ of the adjacent element T. Otherwise, if e is an interior edge, we connect $\mathbf{b}_e$ with the barycenters of the two adjacent elements. This construction results in a mesh $\mathcal{B}_h$ of polygonal dual cells B_p, see the left picture of Figure 2. The construction in 3D follows the same lines, i.e., we connect in a proper way the barycenter of the faces with the midpoint of the edges and the center of the elements. The facets of the dual cell are planar quadrilaterals which can be further decomposed into two triangles, see the right picture of Figure 2.

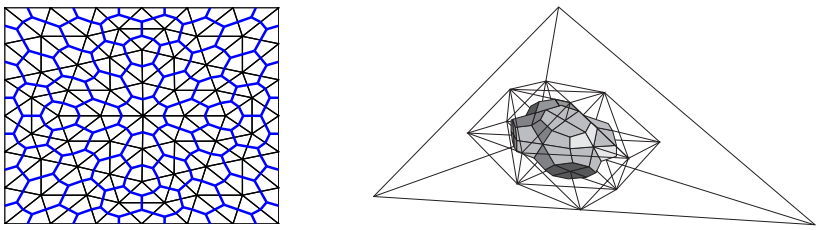

FIG. 2. *Unstructured mesh $\mathcal{T}_h$ in 2D with the associated dual mesh $\mathcal{B}_h$ printed in blue/bold (left) and one dual cell B_p in a structurally refined tetrahedron in 3D (right).*

Denoting by $\mathcal{T}_p$ the set of all elements in $\mathcal{T}_h$ sharing the vertex $\mathbf{p}$, it is easy to verify that

$$\frac{|T|}{d+1} = |B_p^T|, \qquad B_p^T := B_p \cap T, \quad T \in \mathcal{T}_p. \tag{3.1}$$

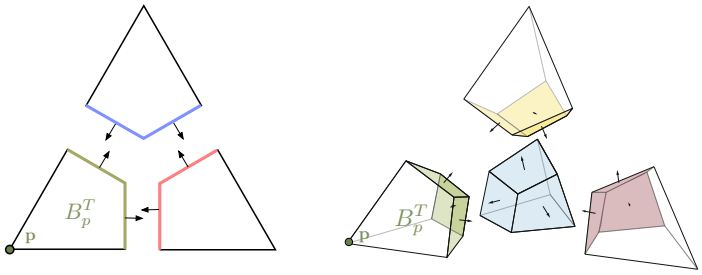

FIG. 3. *Illustration of a dual sub-cell B_p^T in 2D and 3D and oriented normals.*

Our goal is to construct locally conservative mass fluxes on the dual mesh $\mathcal{B}_h$ of the mesh $\mathcal{T}_h$. Each single element $T \in \mathcal{T}_h$ is described by its vertices $\mathbf{p}_i^T$, $i = 1, \dots, d+1$, and with each vertex one dual sub-cell $B_i^T \subset T$ is associated; see Figure 3.

Note that the union of all dual sub-cells associated with the same vertex $\mathbf{p}$ gives the dual cell B_p, and the union of all dual sub-cells associated with the same element T yields the element T; see Figure 4 for an illustration.

To ensure local mass conservation with respect to the dual cells, we would like to define a piecewise constant correction $\kappa_{ij}^T \in P_0(f_{ii}^T)$, where $f_{ij}^T := \partial B_i^T \cap \partial B_j^T$, $1 \le i, j \le d+1$. With each f_{ij}^T we associate a unique normal $\mathbf{n}_{ij}^T$ oriented from B_i^T towards B_j^T. We note that the two faces f_{ij}^T and f_{ji}^T are geometrically the same but have a differently oriented normal; see Figure 3.

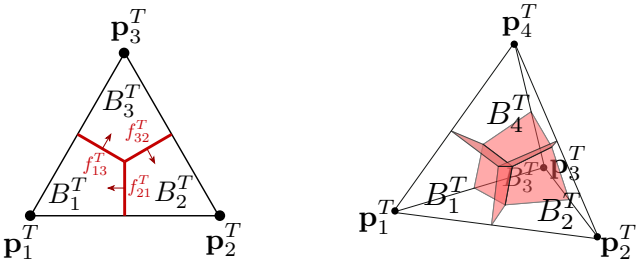

FIG. 4. *Illustration of triangular (left) and tetrahedral (right) element with intersecting barycentric dual boxes and dual facets (in red).*

3.2. Correcting the mass flux on the dual mesh. Given $(\mathbf{u}_h, p_h) \in \mathbf{V}_h \times Q_h$, we define the mass flux defect piecewise as

$$\kappa_{ij}^T(\mathbf{u}_h, p_h) := \frac{1}{(d+1)|f_{ij}^T|}\big(\mathcal{R}_i^T(\mathbf{u}_h, p_h) - \mathcal{R}_j^T(\mathbf{u}_h, p_h)\big), \tag{3.2}$$

where the residuals $\mathcal{R}_i^T$ are defined as

$$\mathcal{R}_i^T(\mathbf{u}_h, p_h) := \int_{B_i^T} \operatorname{div} \mathbf{u}_h \, \mathrm{d}x - \int_T \operatorname{div} \mathbf{u}_h \, \phi_i \, \mathrm{d}x - c_T(p_h, \phi_i) - g_T(p_h, \phi_i),$$

with $\phi_i \in Q_h$ denoting the linear nodal shape function associated with the local vertex i of element $T \in \mathcal{T}_h$. We point out that if $h_Q = h/2$ then ϕ_i is not a nodal

basis function of Q_h but a hierarchical basis function. Finally, we define the oriented mass flux $j(\mathbf{u}_h, p_h)$ face-wise as

$$j(\mathbf{u}_h, p_h)|_{f_{ij}^T} := \mathbf{u}_h|_{f_{ij}^T} \cdot \mathbf{n}_{ij}^T - \kappa_{ij}^T(\mathbf{u}_h, p_h). \tag{3.3}$$

REMARK 3.1. *For a stable pairing with $c_h(\cdot,\cdot) = 0$ and $g_h(\cdot) = 0$, the correction $\kappa_{ij}^T(\mathbf{u}_h, p_h)$ obviously does not depend on p_h, while for $k_V = 1$ and $h_V = h$ the correction does not depend on $\mathbf{u}_h$ since, due to* (3.1)*, the divergence terms cancel inside each element. In Section 4, we will discuss special cases in more detail.*

Given these preparations, we can formulate our main observation.

THEOREM 3.2 (Dual mass conservation). *Let $(\mathbf{u}_h, p_h) \in \mathbf{V}_h \times Q_h$ denote the discrete solution of* (2.1)*. Under the local consistency assumption on the stabilization term*

$$c_T(\cdot, 1) = 0, \quad g_T(1) = 0, \quad T \in \mathcal{T}_h, \tag{3.4}$$

we obtain a local mass conservation on each dual cell

$$\int_{\partial B_p} j(\mathbf{u}_h, p_h)\, \mathrm{d}s = 0, \qquad B_p \in \mathcal{B}_h.$$

Proof. Firstly, we split the flux into the normal velocity and the correction and apply the divergence theorem

$$\int_{\partial B_p} j(\mathbf{u}_h, p_h)\, \mathrm{d}s = \int_{B_p} \operatorname{div} \mathbf{u}_h \, \mathrm{d}x - \sum_{T \in \mathcal{T}_p} \sum_{j=1}^{d} \int_{f_{i_p i_j}^T} \kappa_{i_p i_j}^T(\mathbf{u}_h, p_h)\, \mathrm{d}s, \tag{3.5}$$

where $i_p \in \{1, \dots, d+1\}$ is the local index of the global vertex $\mathbf{p}$ within the element T, $i_j \in \{1, \dots, d+1\} \setminus i_p$ and $\{i_p, i_1, \dots, i_d\} = \{1, \dots, d+1\}$.

In a second step, we consider the correction in more detail. The definition of the flux corrections (3.2) then yields by (2.1b) that

$$\begin{aligned}
&(d+1) \sum_{T \in \mathcal{T}_p} \sum_{j=1}^{d} \int_{f_{i_p i_j}^T} \kappa_{i_p i_j}^T(\mathbf{u}_h, p_h)\, \mathrm{d}s = \\
&\quad = \sum_{T \in \mathcal{T}_p} (d+1) \left(\int_{B_{i_p}^T} \operatorname{div} \mathbf{u}_h \, \mathrm{d}x - \int_T \operatorname{div} \mathbf{u}_h \, \phi_p \, \mathrm{d}x - c_T(p_h, \phi_p) - g_T(p_h, \phi_p) \right) \\
&\qquad + \sum_{T \in \mathcal{T}_p} \sum_{j=1}^{d+1} \left(- \int_{B_j^T} \operatorname{div} \mathbf{u}_h \, \mathrm{d}x + \int_T \operatorname{div} \mathbf{u}_h \, \phi_j \, \mathrm{d}x + c_T(p_h, \phi_j) + g_T(p_h, \phi_j) \right) \\
&\quad = (d+1) \left(\int_{B_p} \operatorname{div} \mathbf{u}_h \, \mathrm{d}x + b(\mathbf{u}_h \, \phi_p) - c_h(p_h, \phi_p) - g_h(p_h, \phi_p) \right) \\
&\qquad + \sum_{T \in \mathcal{T}_p} \left(- \int_T \operatorname{div} \mathbf{u}_h \, \mathrm{d}x + \int_T \operatorname{div} \mathbf{u}_h \, \mathrm{d}x + c_T(p_h, 1) + g_T(p_h, 1) \right) \\
&\quad = (d+1) \int_{B_p} \operatorname{div} \mathbf{u}_h \, \mathrm{d}x.
\end{aligned}$$

In the last step, we employed the assumption (3.4) and the fact that locally on T the functions ϕ_i form a partition of unity, i.e., $\sum_{i=1}^{d+1} \phi_i = 1$. Using the resulting expression in (3.5) yields local mass conservation on the dual cell B_p. ∎

3.3. Strong mass conservation. Each dual box can be decomposed into a fixed bounded number of triangles in 2D and of tetrahedra in 3D resulting globally in a suitably chosen simplicial sub-mesh $\mathcal{T}_{h_s}$ such that each element of the velocity mesh can be written as a union of elements of this sub-mesh. This sub-mesh can be associated with a $\mathbf{H}(\mathrm{div},\Omega)$-conforming discrete space, and we can construct a post-processed solution which is strongly divergence-free. Let $\mathbf{W}_h := \{\mathbf{w}_h \in \mathbf{H}(\mathrm{div};\Omega);\ \mathbf{w}_h|_T \in \mathbb{RT}_{k_V-1}(T),\ T \in \mathcal{T}_{h_s}\}$, where $\mathbb{RT}_k(T)$ denotes the local Raviart–Thomas space of degree $k \geq 0$. Our post-processed solution has the form $\widetilde{\mathbf{u}}_h = \mathbf{u}_h + \mathbf{E}\kappa$, where $\mathbf{E}\kappa \in \mathbf{W}_h$. The extension $\mathbf{E}\kappa$ lifts the face correction $\kappa_{ij}^T(\mathbf{u}_h, p_h)$ and is obtained locally on each dual box by solving a small problem. Let f_{ij}^T be a face of the dual box B_p such that the outer unit normal of B_p on this face is equal to $\mathbf{n}_{ij}^T$. Then we define $\mathbf{E}\kappa$ by the following two steps. Firstly, we set

$$\mathbf{E}\kappa|_{f_{ij}} \cdot \mathbf{n}_{ij}^T := \kappa_{ij}^T(\mathbf{u}_h, p_h)$$

for all faces of B_p. Secondly, we define $\mathbf{E}\kappa$ in the interior of the dual box by

$$\mathrm{div}\, \mathbf{E}\kappa|_{B_p} := -\ \mathrm{div}\, \mathbf{u}_h|_{B_p} \tag{3.6a}$$

$$\|\mathbf{E}\kappa\|_{0;B_p} \leq \|\mathbf{E}\kappa + \mathbf{w}_0\|_{0;B_p}, \tag{3.6b}$$

for all $\mathbf{w}_0 \in \mathbf{W}_h$ such that $\mathrm{supp}\ \mathbf{w}_0 \subset \overline{B}_p$ and $\mathrm{div}\, \mathbf{w}_0 = 0$. We note that Theorem 3.2 guarantees that $\mathbf{E}\kappa$ is well-defined, and by (3.6a) it is obvious that $\widetilde{\mathbf{u}}_h$ is strongly divergence free. A discrete norm equivalence [7] and a straightforward computation then shows that

$$\|\mathbf{E}\kappa\|_0^2 \leq C \left(h^2 \| \mathrm{div}\, \mathbf{u}_h\|_0^2 + \sum_T |T| \sum_{1\leq i<j\leq d+1} (\kappa_{ij}^T(\mathbf{u}_h, p_h))^2 \right). \tag{3.7}$$

The following theorem states that under some mild consistency assumptions of the stabilization terms, the a priori convergence order of $\widetilde{\mathbf{u}}_h$ in the L^2-norm is the same as the one of $\mathbf{u}_h$.

THEOREM 3.3 (A priori order). *Let $(\mathbf{u}_h, p_h) \in \mathbf{V}_h \times Q_h$ denote the discrete solution of* (2.1) *and $\widetilde{\mathbf{u}}_h$ the locally post-processed mixed finite element. Let the a priori estimate* (2.6) *hold. Then under the local consistency order assumption on the stabilization term for $p \in H^k(\Omega)$*

$$\sum_{T\in\mathcal{T}_h} \sum_{i=1}^{d+1} \frac{|c_T(\Pi_h p, \phi_i) + g_T(\phi_i)|^2}{\|\phi_i\|_{0;T}^2} = \mathcal{O}(h^{2k}), \tag{3.8}$$

we obtain $\|\mathbf{u} - \widetilde{\mathbf{u}}_h\|_0 = \mathcal{O}(h^{k+1})$.

Proof. The a priori bound (2.6), the triangle inequality and the stability estimate (3.7) for $\mathbf{E}\kappa$ show that it is sufficient to bound $\kappa_{ij}^T(\mathbf{u}_h, p_h)$ in a proper way. Using the definition (3.2) and the stability assumption on $c_T(\cdot,\cdot)$, we find

$$\begin{aligned} |T| \sum_{1\leq i<j\leq d+1} \kappa_{ij}^T(\mathbf{u}_h, p_h)^2 \ &\leq\ C \frac{h_T^2}{|T|} \sum_{i=1}^{d+1} \mathcal{R}_i^T(\mathbf{u}_h, p_h)^2 \\ &\leq Ch^2 \left(\| \mathrm{div}\, \mathbf{u}_h\|_{0;T}^2 + \|p_h - \Pi_h p\|_{0;T}^2 + \sum_{i=1}^{d+1} \frac{|c_T(\Pi_h p, \phi_i) + g_T(\phi_i)|^2}{\|\phi_i\|_{0;T}^2} \right). \end{aligned}$$

Summing over all $T \in \mathcal{T}_h$ and using the consistency order assumption (3.8) yields the stated a priori estimate. ∎

3.3.1. Implementation aspects. The sub-mesh $\mathcal{T}_{h_s}$ aims to be a refinement of both, the primal mesh $\mathcal{T}_h$, and the dual mesh $\mathcal{B}_h$. While this construction is favorable for the analysis, it is not very suitable for implementation. For practical purposes it is more convenient to define the lifting to strongly mass-conservative spaces with respect to the mesh $\mathcal{T}_{h/2}$ which is a uniform refinement of $\mathcal{T}_h$. We will thus present an alternative construction that lifts the velocity in a computationally inexpensive fashion, such that the order of convergence of the original scheme is preserved. We again proceed in two steps: Firstly, we can determine a lifting of the flux-corrections to the lowest-order Raviart-Thomas space $\Pi_{T\in\mathcal{T}_{h/2}}\mathbb{RT}_0(T)\cap\mathbf{H}(\mathrm{div};\Omega)$, which requires the solution of small problems on the sub-triangulations associated with each dual box. Secondly, for $k_V>1$, we can incorporate (3.6a) locally on each $T\in\mathcal{T}_{h/2}$ by determining the coefficients of the interior moments of $\mathbb{RT}_{k_V-1}(T)$. This is again a computationally inexpensive procedure, since the normal components of the interior ansatz functions vanish at ∂T and hence couple only locally. Let us briefly discuss how we could obtain facet-wise flux-corrections with respect to $\mathcal{T}_{h/2}$ in a practical implementation. We work out the details only for the 2D case; the 3D case is technical and requires more notation but follows by essentially the same arguments. For further reading, we refer to the finite element literature on local flux-equilibration, cf. e.g., [1, 34, 29] and the references cited therein.

We start with the construction of the sub-mesh $\mathcal{T}_{h_s}$. Each element $T\in\mathcal{T}_h$ is decomposed into six sub-elements in the following way. Firstly T is refined uniformly by connecting the midpoints of the edges. This gives us four sub-elements. Secondly the center sub-element which does not contain a vertex of the original element T is further decomposed into three sub-elements by connecting its vertices with the barycenter of the original element T. We point out that by this construction $\mathcal{T}_{h_s}$ is not only a sub-mesh of $\mathcal{T}_h$ but also of $\mathcal{T}_{h/2}$.

As we can see in Figure 5, a dual box $B_p\in\mathcal{B}_h$ is geometrically composed of the patch of elements $\mathcal{T}_{h/2}^p$ sharing all the same macro mesh node $\mathbf{p}\in\mathcal{P}_h$ and additional triangles T_i, which are defined by the edges $e_i\in\mathcal{E}_{h/2}$ opposing the vertex p and the barycenter of the element neighboring at this edge. Here, $\mathcal{E}_{h/2}$ denotes the set of edges of $\mathcal{T}_{h/2}$. Thus each dual box can be written as union of elements of the sub-mesh $\mathcal{T}_{h_s}$. Since we already established a conservative flux $j(\mathbf{u}_h,p_h)$ on the boundaries of the dual cells, we can proceed locally for the edges contained in B_p. Similar to (3.3), we define

$$j(\mathbf{u}_h,p_h)|_{\partial T\cap e}:=\mathbf{u}_h\cdot\mathbf{n}|_e-\kappa_e^T(\mathbf{u}_h,p_h)\quad\text{on}\quad T\in\mathcal{T}_{h/2},\quad e\in\mathcal{E}_{h/2}. \tag{3.9}$$

Our first observation is that we can locally equilibrate the fluxes on the elements T_i. Since we are missing one flux-correction $\kappa(\mathbf{u}_h)|_{e_i}\in P_0(e_i)$ on each e_i, we form the local mass balance

$$\int_{\partial T_i} j(\mathbf{u}_h,p_h)\,\mathrm{d}s\overset{!}{=}0,$$

and explicitly solve for $\kappa_{e_i}^T(\mathbf{u}_h,p_h)$; cf. Figure 5 (left). This is easy, since we already have conservative fluxes defined on two of three edges of T_i by the construction of the previous section. Hence, the problem reduces to determining flux-corrections on the interior edges of the patch of elements $\mathcal{T}_{h/2}^p$. Let us outline the procedure, which is similar to the construction in [1, Sect. 6.4.5]. For each interior node $\mathbf{p}\in\mathcal{P}_h$, we have $n=|\mathcal{T}_{h/2}^p|=|\mathcal{E}_{h/2}^p|$, which generates a linear problem of the form

$$\mathbf{L}\boldsymbol{\kappa}=\mathbf{r}, \tag{3.10}$$

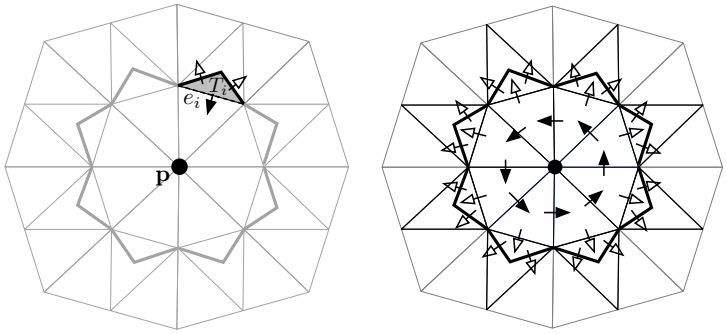

FIG. 5. *Oriented flux-corrections associated with a triangle T_i and an edge e_i (left) and with an entire dual cell (bold line) for $n = |\mathcal{T}_{h/2}^p| = 8$ (right). The $3n$ empty arrows in the right illustration denote quantities which can be explicitly computed from $\mathbf{u}_h$, and the n filled arrows denote degrees of freedom which need to be determined by solving a local $n \times n$ problem.*

with n unknowns and n equations. Here, the rows $\mathbf{L}_k$ and $\mathbf{r}_k$ are associated with the mass-balance over the boundary of one element in $\mathcal{T}_{h/2}^p$, and $\boldsymbol{\kappa}$ is the vector containing the values $\kappa_e^{T_k}(\mathbf{u}_h, p_h)|e|$, $e \in \mathcal{E}_{h/2}^p$. For each $T_k \in \mathcal{T}_{h/2}^p$ the mass-balance can be written as

$$0 \overset{!}{=} \int_{\partial T_k} j(\mathbf{u}_h, p_h)\,\mathrm{d}s \quad \Leftrightarrow \quad \sum\nolimits_{e \subset \partial T_k} \kappa_e^{T_k}(\mathbf{u}_h, p_h)|e| = \operatorname{div} \mathbf{u}_h|_{T_k}|T_k|.$$

Assuming a counter-clockwise ordering of degrees of freedom inside the element patch as depicted in Figure 5, this leaves us with solving a system of the form:

$$\underbrace{\begin{pmatrix} -1 & 1 & 0 & \dots & 0 & 0 \\ 0 & -1 & 1 & \dots & 0 & 0 \\ 0 & 0 & -1 & \dots & 0 & 0 \\ \vdots & \vdots & \vdots & \vdots & \ddots & \vdots \\ 0 & 0 & 0 & \dots & -1 & 1 \\ 1 & 0 & 0 & \dots & 0 & -1 \end{pmatrix}}_{\mathbf{L}} \cdot \underbrace{\begin{pmatrix} \kappa_1 \\ \kappa_2 \\ \kappa_3 \\ \vdots \\ \kappa_{n-1} \\ \kappa_n \end{pmatrix}}_{\boldsymbol{\kappa}} = \underbrace{\begin{pmatrix} r_1 \\ r_2 \\ r_3 \\ \vdots \\ r_{n-1} \\ r_n \end{pmatrix}}_{\mathbf{r}}. \tag{3.11}$$

The operator $\mathbf{L}$ has a non-trivial kernel $\ker \mathbf{L} = \operatorname{span}\{\mathbf{1}\}$, where $\mathbf{1} := [1, 1, \dots, 1]^\top$, since we can add any constant to each of the corrections in the interior of the patch and still obtain locally conservative fluxes. This implies that a solution to (3.10) exists if and only if $\mathbf{1}^\top \cdot \mathbf{r} = 0$, which can be easily verified by substituting the definition of $\mathbf{r}$ and using the conservation properties derived above. For reconstructing unique flux-corrections inside each patch of elements, we do not follow (3.6b). Instead of minimizing the L^2-norm, we minimize the Euclidean norm, i.e., we find

$$\min_{\boldsymbol{\kappa} \in \mathbb{R}^n} |\boldsymbol{\kappa}|_2, \quad \text{such that} \quad \mathbf{L}\boldsymbol{\kappa} = \mathbf{r}.$$

This procedure is a simplification of (3.6b) and computational cheaper. Due to a discrete norm equivalence the bound of Theorem 3.3 still holds.

For the dual cells located at the boundary we have no circular dependencies. Hence, the local system is uniquely solvable as long as we have one edge at a Dirichlet

boundary. For cells located at a pure Neumann boundary, a similar procedure as for the interior cells needs to be carried out.

REMARK 3.4 (Possible extensions). *The proof of the mass conservation of the post-processed flux only exploits the fact that suitably selected functions of Q_h form locally a partition of unity and that the dual sub-cells decompose the elements. Thus it is possible to apply these type of arguments to more general meshes and other type of finite elements, e.g., quadrilateral meshes and bilinear velocity elements. Let us finally remark that the generalization towards other types of incompressible flow problems such as the Navier–Stokes equations is straightforward. In particular, the way in which we obtain conservative mass-fluxes is independent of the exact form of the momentum equation since it only relies on abstract requirements on the stabilizing operator. Using a suitable transformation of the momentum equation in terms of the mass flow rate per area $\mathbf{w} := \rho\mathbf{u}$, where ρ denotes a spatially varying fluid density, the exact mass-conservation $\operatorname{div}\mathbf{w} = 0$ can even be achieved in this way for compressible Stokes models, which are widely used, e.g., in mantle convection simulations.*

4. Stabilized linear finite elements. In this section, we focus on stabilized equal-order finite element approximations with $k_V = 1 = k_Q$. Let us first consider the popular case $h_V = h = h_Q$. In Remark 3.1, we already stated that for the equal-order linear ansatz spaces it is in fact the presence of the additional stabilization terms which destroys local mass-conservation, and thus the correction has to compensate for the effects introduced here. There exists a variety of well-established stabilization techniques, which are typically based on Petrov–Galerkin formulations, artificial compressibility, interior-penalty or additional projection-terms; cf., e.g., [12, 4, 9, 6, 35, 23, 33, 3, 7] for an overview. While several of the above cited works deal with stabilizations that satisfy the assumption (3.4) (or a patch-wise variant thereof), we would like to focus on two popular stabilization approaches below which are widely used in CFD codes, namely the pressure-stabilized Petrov–Galerkin (PSPG) scheme [12, 31, 43] and a projection-based stabilization due to Bochev, Dohrmann, and Gunzburger [6] which we refer to as BDG stabilization.

4.1. The PSPG stabilization. The PSPG-scheme stabilizes the equal-order finite-element spaces by choosing

$$c_h(p,q) := \sum_{T\in\mathcal{T}_h} \delta_T \int_T \nabla p\cdot\nabla q\,\mathrm{d}x, \tag{4.1}$$

where $\delta_T := \alpha_T\, h_T^2$ scales with the local element diameter for some carefully chosen constant α_T; cf., e.g., [41, 4, 22] for details. For the residual-based PSPG scheme a consistency term $g_h(q) = -\sum_{T\in\mathcal{T}_h}\delta_T\int_T \mathbf{f}\cdot\nabla q\,\mathrm{d}x$ may be added on the right hand side if $\mathbf{f}\neq 0$; see [31]. Moreover, since the stabilization acts as a Neumann condition on the pressure, thereby causing problems in the presence of Dirichlet boundaries, Droux and Hughes proposed the inclusion of a non-symmetric interface consistency term for p; cf. [19]. In practice, these modifications neither influence the stability nor the asymptotic rate of convergence of the method. However they can have a significant influence on the quality of the pressure solution. In our setting, these additional terms would of course have to be considered in the construction of flux-corrections but they only involve integrals which have to be computed for the local assembly of the stiffness matrices anyway. Since these terms otherwise do not interfere with our arguments, we ignore such modifications below to simplify our presentation and assume $g_T(\cdot) = 0$. It

is obvious, that the assumptions on the stabilization term, in particular, (2.4), (2.5), (3.4), and (3.8), are satisfied. Thus we are in the settings of Theorems 3.2 and 3.3.

LEMMA 4.1. *In the case of the PSPG stabilization* (4.1) *with* $g_h(\cdot) = 0$*, the flux correction has the simple form*

$$\kappa_{ij}^T(p_h) = \delta_T \nabla p_h|_T \cdot \mathbf{n}_{ij}^T. \tag{4.2}$$

Proof. We use a well-known equivalence between finite-element and finite-volume discretizations of diffusion operators which gives $\int_T \nabla p_h \cdot \nabla \phi_i = -\int_{\partial B_i \cap T} \nabla p_h \cdot \mathbf{n}$; cf., e.g., [32, Lemma 6.11]. By this we find that the flux-correction given by (3.2) can be rewritten as

$$\begin{aligned}
\kappa_{ij}^T(\mathbf{u}_h, p_h) = \kappa_{ij}^T(p_h) &= \frac{1}{(d+1)|f_{ij}^T|}\big(c_T(p_h, \phi_j) - c_T(p_h, \phi_i)\big) \\
&= \frac{\delta_T}{(d+1)|f_{ij}^T|} \int_T \nabla p_h \cdot \nabla(\phi_j - \phi_i)\,\mathrm{d}x \\
&= \frac{\delta_T}{(d+1)|f_{ij}^T|} \left(\int_{\partial B_i \cap T} \nabla p_h \cdot \mathbf{n}_{ij}^T\,\mathrm{d}x - \int_{\partial B_j \cap T} \nabla p_h \cdot \mathbf{n}_{ji}^T\,\mathrm{d}x \right).
\end{aligned}$$

Now we discuss the cases $d = 2$ and $d = 3$ separately. We start with $d = 2$ and set the index k such that $\{i, j, k\} = \{1, 2, 3\}$. Using $\mathbf{n}_{ij}^T = -\mathbf{n}_{ji}^T$ and $|f_{ij}^T| = |f_{ji}^T|$, we get

$$\begin{aligned}
\int_{\partial B_i \cap T} \nabla p_h \cdot \mathbf{n}_{ij}^T\,\mathrm{d}x - \int_{\partial B_j \cap T} \nabla p_h \cdot \mathbf{n}_{ji}^T\,\mathrm{d}x &= \nabla p_h|_T \cdot \big(2\mathbf{n}_{ij}^T|f_{ij}^T| + \mathbf{n}_{ik}^T|f_{ik}^T| - \mathbf{n}_{jk}^T|f_{jk}^T|\big) \\
&= 3\nabla p_h|_T \cdot \mathbf{n}_{ij}^T|f_{ij}^T| + \nabla p_h|_T \cdot \big(\mathbf{n}_{ji}^T|f_{ji}^T| + \mathbf{n}_{ik}^T|f_{ik}^T| + \mathbf{n}_{kj}^T|f_{kj}^T|\big) \\
&= 3\nabla p_h|_T \cdot \mathbf{n}_{ij}^T|f_{ij}^T| = (d+1)|f_{ij}^T|(\nabla p_h|_T \cdot \mathbf{n}_{ij}^T).
\end{aligned}$$

The terms in the second but last step cancel due to the fact that for a triangle

$$\sum\nolimits_{i=1}^3 (\mathbf{b}_T - \mathbf{b}_{e_i}) = \mathbf{0}, \tag{4.3}$$

where $\mathbf{b}_T$ is the element barycenter, and $\mathbf{b}_{e_i}$ are the edge-midpoints; see Figure 6.

The case $d = 3$ involves more notation but follows basically the same lines. For $i \neq j$ fixed, we define $i_1 = j$ and i_2, i_3 such that $\{i, i_1, i_2, i_3\} = \{1, 2, 3, 4\}$ and $(\mathbf{p}_{i_3}^T - \mathbf{p}_i^T)^\top \cdot ((\mathbf{p}_{i_1}^T - \mathbf{p}_i^T) \times (\mathbf{p}_{i_2}^T - \mathbf{p}_i^T)) > 0$ holds, and we set $j_1 = i$, $j_2 = i_3$ $j_3 = i_2$. In terms of this notation, we find

$$\begin{aligned}
\int_{\partial B_i \cap T} \nabla p_h \cdot \mathbf{n}_{ij}^T\,\mathrm{d}x - \int_{\partial B_j \cap T} \nabla p_h \cdot \mathbf{n}_{ji}^T\,\mathrm{d}x &= \nabla p_h|_T \cdot \sum_{l=1}^3 \big(\mathbf{n}_{ii_l}^T|f_{ii_l}^T| - \mathbf{n}_{jj_l}^T|f_{jj_l}^T|\big) \\
&= 4\nabla p_h|_T \cdot \mathbf{n}_{ij}^T|f_{ij}^T| + \nabla p_h|_T \cdot \sum_{l=2}^3 \big(\mathbf{n}_{ii_l}^T|f_{ii_l}^T| - \mathbf{n}_{jj_l}^T|f_{jj_l}^T| - \mathbf{n}_{ij}^T|f_{ij}^T|\big).
\end{aligned}$$

To show that (4.2) holds, we have to consider $\sum_{l=2}^3 \big(\mathbf{n}_{ii_l}^T|f_{ii_l}^T| - \mathbf{n}_{jj_l}^T|f_{jj_l}^T| - \mathbf{n}_{ij}^T|f_{ij}^T|\big)$ in more detail. Let $\mathbf{b}_{e_{lk}} = \mathbf{b}_{e_{kl}}$ be the midpoint of the edge between the vertices $\mathbf{p}_l^T$ and $\mathbf{p}_k^T$, $l \neq k$, $l, k \in \{1, 2, 3, 4\}$, $\mathbf{b}_T$ the barycenter of the tetrahedra and $\mathbf{b}_{f_k}$ the center of the face which does not contain the vertex $\mathbf{p}_k^T$, $k \in \{1, 2, 3, 4\}$. Then we have the elementary relations

$$\mathbf{n}_{ij}^T|f_{ij}^T| = \tfrac{1}{2}(\mathbf{b}_T - \mathbf{b}_{e_{ij}}) \times (\mathbf{b}_{f_{i_2}} - \mathbf{b}_{f_{i_3}}), \tag{4.4}$$

cf. Figure 6, and $\mathbf{b}_T - \mathbf{b}_{e_{ij}} = \frac{3}{4}(\mathbf{b}_{f_i} + \mathbf{b}_{f_j} - \mathbf{b}_{f_{i_2}} - \mathbf{b}_{f_{i_3}})$. Exploiting the relation between the weighted normals and the cross-product formula for all index pairings and using $\mathbf{a} \times \mathbf{b} = -\mathbf{b} \times \mathbf{a}$, and $\mathbf{a} \times \mathbf{a} = \mathbf{0}$, we obtain $\sum_{l=2}^{3} \left(\mathbf{n}_{ii_l}^T |f_{ii_l}^T| - \mathbf{n}_{jj_l}^T |f_{jj_l}^T| - \mathbf{n}_{ij}^T |f_{ij}^T| \right) = \mathbf{0}$ which ends the proof. □

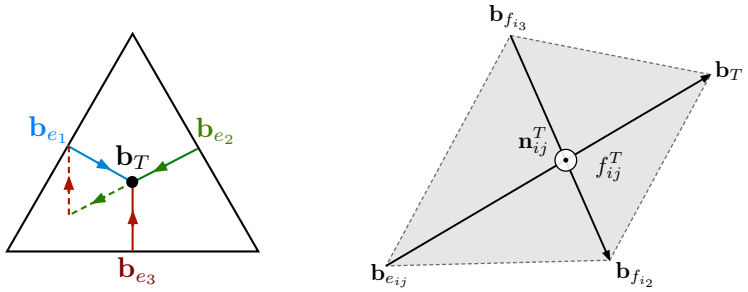

FIG. 6. *Illustration of relations* (4.3) *and* (4.4).

4.2. The BDG stabilization. The BDG-stabilization [6] is based on local projection terms, i.e., we choose

$$c_h(p,q) := \sum_{T \in \mathcal{T}_h} \alpha_0 \int_T (p - \Pi_0 p)(q - \Pi_0 q) \, \mathrm{d}x, \tag{4.5}$$

where Π_0 is the (locally defined) projection onto piecewise constants, which can be realized if p is affine of T, e.g., by evaluation at element barycenters $\mathbf{b}_T$. Again, the assumptions on the stabilization term, in particular (2.4), (2.5), (3.4), and (3.8), are obviously satisfied. Hence, the settings of Theorems 3.2 and 3.3 apply.

LEMMA 4.2. *For the BDG stabilization* (4.5)*, the flux correction simplifies to*

$$\kappa_{ij}^T(p_h) = \frac{\alpha_0 |T| (p_j - p_i)}{(d+1)^2 (d+2) |f_{ij}^T|}.$$

Proof. By (3.2) the flux can be written as

$$\begin{aligned} \kappa_{ij}^T(\mathbf{u}_h, p_h) = \kappa_{ij}^T(p_h) &= \frac{\alpha_0}{(d+1)|f_{ij}^T|} \int_T p_h(\phi_j - \phi_i - \Pi_0(\phi_i - \phi_j)) \, \mathrm{d}x \\ &= \frac{\alpha_0}{(d+1)|f_{ij}^T|} \sum_{k=1}^{d+1} p_k^T \int_T \phi_k(\phi_j - \phi_i) \, \mathrm{d}x, \end{aligned}$$

where p_k^T denotes the local pressure coefficients of element T. In the last step, we used that $\Pi_0(\phi_i - \phi_j) = 0$ for i, j simplex vertices and ϕ_i, ϕ_j the associated shape functions. This form is already suitable for implementation, since the evaluation of the integral only involves the difference of element coefficients weighted by entries of the mass matrix. Moreover, by computing the entries explicitly, we find that $\int_T \phi_i \phi_j \, \mathrm{d}x = |T|(1 + \delta_{ij}) \frac{d!}{(d+2)!}$, hence we can further simplify as

$$\kappa_{ij}^T(p_h) = \frac{\alpha_0 |T|}{(d+1)^2 (d+2) |f_{ij}^T|} \sum_{k=1}^{d+1} p_k^T (\delta_{kj} - \delta_{ki}) = \frac{\alpha_0 |T| (p_j - p_i)}{(d+1)^2 (d+2) |f_{ij}^T|},$$

which proves the assertion. □

Again, we observe that the corrections resemble scaled normal derivatives of the pressure, although, of course, on general meshes a scaled tangential derivative along an edge does not exactly correspond to the normal gradient of p_h on f_{ij}^T. This is no coincidence, since many different stabilization schemes are strongly related in the sense that they add additional scaled pressure-Laplacians on a discrete level; e.g., the BDG stabilization can be interpreted as a PSPG scheme with piecewise constant anisotropic stabilization tensors instead of scalar constants.

4.3. The two-level stabilization. In this section, we discuss a case such that the flux correction only depends on the velocity. Using the abstract results of the previous section, we construct step by step the correction for the cases $k_V = 1 = k_Q$ and $h_V = h/2$, $h_Q = h$, or $k_V = 1 = k_Q$ and $h_V = h/2 = h_Q$. These cases are somehow more involved than the previously considered linear-linear schemes since we have to work with two mesh levels and the cells of the corresponding dual meshes are non-nested, see Figure 7. The first pairing is stable and the latter is stabilized

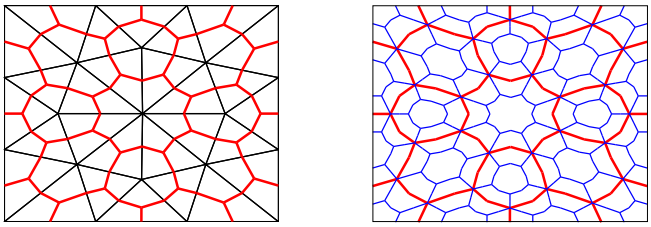

FIG. 7. *Example of an unstructured mesh $\mathcal{T}_h$ and its dual mesh $\mathcal{B}_h$ (left) and the overlap of the dual meshes $\mathcal{B}_h$ and $\mathcal{B}_{h/2}$ (right).*

by a two-level approach. Here we use a form which can be cheaply realized within a geometric multigrid solver and define the stabilization form in terms of an operator which can be implemented as an injection to the mesh $\mathcal{T}_h$ followed by a prolongation onto the mesh $\mathcal{T}_{h/2}$. Given the nodal interpolation operator I_h from the mesh $\mathcal{T}_{h/2}$ onto the mesh $\mathcal{T}_h$, we set for $p, q \in Q_h$

$$c_h(p,q) := \alpha_1 \int_\Omega (p - I_h p)(q - I_h q)\,\mathrm{d}x, \quad g_h(p) = 0. \tag{4.6}$$

It is obvious that the following abstract properties for I_h hold:

$$I_h q|_T = q|_T, \qquad \text{if } q \in Q_h \text{ and } q|_T \in P_1(T), T \in \mathcal{T}_h \tag{4.7a}$$

$$\|I_h q\|_0 \le \gamma_s \|q\|_0, \qquad q_h \in Q_h. \tag{4.7b}$$

Since, due to (4.7a), the kernel of the discrete operator associated with c_h is exactly the conforming finite element space associated with the mesh $\mathcal{T}_h$, we only penalize the checkerboard modes which are the cause of pressure instabilities in equal-order methods; see Figure 8 for some illustration.

REMARK 4.3. *Similar stabilizations are considered in [41, 42], and the flux correction procedure outlined below carries over straightforwardly also to other two-level approaches provided that the Q_h is a subset of the kernel of the stabilizing operator.*

4.3.1. Uniform stability and convergence. For the sake of completeness, we briefly revise the proof that the stability assumption (2.3) holds. As an important

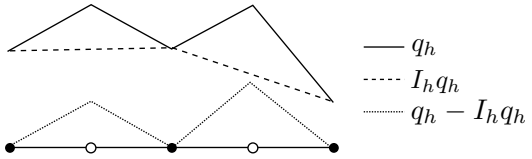

FIG. 8. *Illustration of the action of the stabilization operator in 1D.*

ingredient for the following analysis, we first recall the fact that $\mathbf{V}_h \times Q_H^0$ forms a uniformly stable pairing [5, 24]. Here $Q_H^0 := \{q \in H^1(\Omega), q|_T \in P_1(T), T \in \mathcal{T}_h\} \cap L_0^2(\Omega)$. We recall that in this section Q_h and V_h are associated with the finer mesh $\mathcal{T}_{h/2}$. Let $\beta_{\mathrm{s}} > 0$ be the uniform inf-sup constant of the pairing $\mathbf{V}_h \times Q_H^0$, and $\beta_{\mathrm{c}} > 0$ be the uniform coercivity constant of $a(\cdot,\cdot)$ with respect to the H^1-Norm, i.e.,

$$\inf_{q_H \in Q_H^0} \sup_{\mathbf{v}_h \in \mathbf{V}_h} \frac{b(\mathbf{v}_h, q_H)}{a(\mathbf{v}_h, \mathbf{v}_h)^{1/2} \|q_H\|_0} \geq \beta_{\mathrm{s}}, \tag{4.8a}$$

$$a(\mathbf{v}_h, \mathbf{v}_h)^{1/2} \geq \beta_{\mathrm{c}} \|\mathbf{v}_h\|_1, \quad \mathbf{v}_h \in \mathbf{V}_h. \tag{4.8b}$$

LEMMA 4.4. *For $\alpha > 0$ the discrete Stokes formulation* (2.2) *is uniformly stable, i.e., there exists a stability constant $\gamma_c > 0$ independent of h such that*

$$\sup_{\mathbf{v}_h \in \mathbf{V}_h} \sup_{q_h \in Q_h^0} \frac{S_h(\mathbf{w}_h, r_h; \mathbf{v}_h, q_h)}{\|(\mathbf{v}_h, q_h)\|} \geq \gamma_c \|(\mathbf{w}_h, r_h)\|, \quad \mathbf{w}_h \in \mathbf{V}_h,\ r_h \in Q_h^0.$$

Moreover the stability constant γ_c depends only on γ_s, β_s, β_c and α_1.

Proof. The proof is based on the decomposition $r_h = r_h - (\mathrm{Id} - \Pi_0) I_h r_h + (\mathrm{Id} - \Pi_0) I_h r_h$ and the uniform inf-sup stability (4.8a) over $\mathbf{V}_h \times Q_H^0$. Here Π_0 is the L^2-projection onto $P_0(\Omega)$. For $r_h \in Q_h^0$, we find $r_H := (\mathrm{Id} - \Pi_0) I_h r_h \in Q_H^0$, and thus $\|r_h - r_H\|_0 = \|(\mathrm{Id} - \Pi_0)(r_h - I_h r_h)\|_0 \leq \|r_h - I_h r_h\|_0$. Moreover due to (4.8a), there exists a $\mathbf{z}_h \in \mathbf{V}_h$ such that for $\tau > 0$ fixed there holds

$$a(\mathbf{z}_h, \mathbf{z}_h) = \tau^2 \|r_H\|_0^2, \qquad \text{and} \qquad b(\mathbf{z}_h, r_H) = \beta_{\mathrm{s}} \tau \|r_H\|_0^2.$$

Setting $\mathbf{v}_h = \mathbf{w}_h + \mathbf{z}_h$ and $q_h = -r_h$ and using Young's inequality as well as the definition (4.6), we get in terms of (4.7b) and (4.8b) that

$$\|\mathbf{v}_h\|_1 \leq \|\mathbf{w}_h\|_1 + \|\mathbf{z}_h\|_1 \leq \|\mathbf{w}_h\|_1 + \tfrac{\tau}{\beta_{\mathrm{c}}} \|r_H\|_0 \leq \|\mathbf{w}_h\|_1 + \gamma_{\mathrm{s}} \tfrac{\tau}{\beta_{\mathrm{c}}} \|r_h\|_0.$$

Moreover, we find $S_h(\mathbf{w}_h, r_h; \mathbf{v}_h, q_h)$

$$\begin{aligned}
&= a(\mathbf{w}_h, \mathbf{v}_h) + b(\mathbf{v}_h, r_h) + b(\mathbf{w}_h, q_h) - c_h(r_h, q_h) \\
&= a(\mathbf{w}_h, \mathbf{w}_h) + a(\mathbf{w}_h, \mathbf{z}_h) + b(\mathbf{w}_h, r_h) + b(\mathbf{z}_h, r_h) - b(\mathbf{w}_h, r_h) + c_h(r_h, r_h) \\
&= a(\mathbf{w}_h, \mathbf{w}_h) + a(\mathbf{w}_h, \mathbf{z}_h) + b(\mathbf{z}_h, r_h - r_H) + \beta_{\mathrm{s}} \tau \|r_H\|_0^2 + \alpha_1 \|r_h - I_h r_h\|_0^2 \\
&\geq \tfrac{1}{2} a(\mathbf{w}_h, \mathbf{w}_h) + \big(\beta_{\mathrm{s}} \tau - \tfrac{1}{2} \tau^2 (1 + \tfrac{d}{\alpha_1})\big) \|r_H\|_0^2 + \tfrac{\alpha_1}{2} \|r_h - I_h r_h\|_0^2 \\
&\geq \tfrac{1}{2} a(\mathbf{w}_h, \mathbf{w}_h) + \tau \big(\beta_{\mathrm{s}} - \tfrac{\tau}{2} (1 + \tfrac{d}{\alpha_1})\big) \|r_H\|_0^2 + \tfrac{\alpha_1}{2} \|r_h - r_H\|_0^2.
\end{aligned}$$

Setting $\tau > 0$ small enough and using (4.8b), the uniform stability follows. ∎

Thus the stability assumption (2.3) and the consistency assumptions (2.4) and (2.5) are satisfied and order one a priori estimates for the finite element solution $(\mathbf{u}_h, p_h)$ are granted provided that the solution $(\mathbf{u}, p) \in [H^2(\Omega)]^d \times H^1(\Omega)$. It is also

obvious that the consistency assumption (3.4) is satisfied. We point out that this type of assumption is not satisfied with respect to the elements of the fine mesh $\mathcal{T}_{h/2}$. Thus the abstract construction of Section 3 can be applied on $\mathcal{T}_h$ but not on $\mathcal{T}_{h/2}$. Moreover (3.8) trivially holds since $g_T(\cdot) = 0$ and $c_T(\Pi_h p, \phi_i) = 0$. We recall that ϕ_i is a nodal basis with respect to the mesh $\mathcal{T}_h$ and thus $I_h\phi_i|_T = \phi_i|_T$. Provided we have regularity of the dual problem, we are in the setting of Theorem 3.3 and the post-processed velocity $\widetilde{\mathbf{u}}_h$ approximates $\mathbf{u}$ in the L^2-norm with quadratic order.

4.3.2. Flux correction. Let us next consider the concrete form of the flux correction for the stable or stabilized two-level approaches. In 2D, we find an extremely simple form which only involves the divergence of the discrete velocity.

LEMMA 4.5. *For $d = 2$ let $k_V = 1 = k_Q$. Moreover, let either $h_V = h/2 = h_Q$ and $c_h(\cdot,\cdot)$ as in (4.6) or $h_V = h/2$ and $h_Q = h$ (i.e., the P_1-iso-P_2–P_1 scheme). Then the flux correction simplifies to*

$$\kappa_{ij}^T(\mathbf{u}_h) = \frac{|T|}{24|f_{ij}^T|}\left(\operatorname{div}\mathbf{u}_h|_{T_i} - \operatorname{div}\mathbf{u}_h|_{T_j}\right).$$

Moreover, if $\mathbf{u}_h|_T \in P_1(T)$ for some $T \subset \mathcal{T}_h$, then $\kappa_{ij}^T(\mathbf{u}_h) = 0$.

Proof. Let us recall that every triangle $T \in \mathcal{T}_h$ is subdivided into four congruent subtriangles $\mathcal{T}_{h/2}(T) \subseteq \mathcal{T}_{h/2}$. For convenience, we denote the three elements associated with the vertices $\mathbf{p}_k^T \in \mathcal{P}_h$ by T_k, $k = 1, 2, 3$, and the remaining interior element is denoted by T_4. Our starting point is the general definition (3.2) which slightly simplifies for the two-level stabilization:

$$\kappa_{ij}^T(\mathbf{u}_h) = \frac{1}{(d+1)|f_{ij}^T|}\left(\int_{B_i^T}\operatorname{div}\mathbf{u}_h\,\mathrm{d}x - \int_{B_j^T}\operatorname{div}\mathbf{u}_h\,\mathrm{d}x - \int_T \operatorname{div}\mathbf{u}_h(\phi_i-\phi_j)\,\mathrm{d}x\right).$$

For the first part, since the divergence in the interior triangle is constant, we have

$$\int_{B_i^T}\operatorname{div}\mathbf{u}_h\,\mathrm{d}x - \int_{B_j^T}\operatorname{div}\mathbf{u}_h\,\mathrm{d}x = |T_i|\operatorname{div}\mathbf{u}_h|_{T_i} - |T_j|\operatorname{div}\mathbf{u}_h|_{T_j}.$$

To simplify the remaining term, we observe that we can express the integral as

$$\int_T \operatorname{div}\mathbf{u}_h(\phi_i-\phi_j)\,\mathrm{d}x = \sum_{T_k\in\mathcal{T}_{h/2}(T)} |T_k|\operatorname{div}\mathbf{u}_h|_{T_k}(\phi_i(\mathbf{b}_{T_k}) - \phi_j(\mathbf{b}_{T_k})),$$

where again $\mathbf{b}_{T_k}$ denotes the barycenter of T_k. We note that due to symmetry, the terms not involving T_i and T_j cancel. Evaluating the remaining terms yields

$$\begin{aligned}
&\int_T \operatorname{div}\mathbf{u}_h(\phi_i-\phi_j)\,\mathrm{d}x\\
&\quad= |T_i|\operatorname{div}\mathbf{u}_h|_{T_i}(\phi_i(\mathbf{b}_{T_i}) - \phi_j(\mathbf{b}_{T_i})) + |T_j|\operatorname{div}\mathbf{u}_h|_{T_j}(\phi_i(\mathbf{b}_{T_j}) - \phi_j(\mathbf{b}_{T_j}))\\
&\quad= \frac{1}{2}\left(|T_i|\operatorname{div}\mathbf{u}_h|_{T_i} - |T_j|\operatorname{div}\mathbf{u}_h|_{T_j}\right).
\end{aligned}$$

Next, notice that for the subtriangles there holds $|T_i| = |T_j| = \frac{1}{4}|T|$ by construction which concludes the proof. ∎

REMARK 4.6. *For $d = 3$ each uniformly refined tetrahedron consist of eight subtetrahedra of equal volume, namely four congruent subtetrahedra located at the vertices*

and an interior octahedron which is split into four subtetrahedra by introducing a diagonal edge. Hence we are not in the comfortable situation as for $d = 2$, where the interior is only composed of one element. Thus, one can check that the interior contributions do not cancel in general. However, the flux correction can again be expressed as the sum of weighted divergence-differences, where the weights depend on whether the interior diagonal intersects with the dual face or not. The resulting correction formulas follow straightforwardly by geometric arguments but their definition is lengthy and thus not given here for the sake of brevity.

5. Numerical examples. In this section, we complement our theoretical considerations by numerical experiments to highlight the importance of locally mass-conservative velocity fields. Since the effects are most visible for lower order discretizations, we focus on linear finite elements and demonstrate the exact local conservation for different stable and stabilized methods. Moreover, we couple our finite-element solver to a finite-volume code to visibly demonstrate the effects caused by spurious sources and sinks in coupled flow-transport applications, which can be avoided by the proposed postprocessing.

5.1. Colliding flow benchmark. The first test problem is concerned with the *colliding-flow* benchmark on the unit square $\Omega = (-1, 1)^2$ which is used in, e.g.,[37, 4] for comparing low-order methods. Boundary conditions are chosen, such that the exact solution is given by

$$\mathbf{u}(\mathbf{x}) = \left(20xy^3, 5x^4 - 5y^4\right), \quad \text{and} \quad p(\mathbf{x}) = 60x^2y - 20y^3, \qquad \mathbf{x} := (x, y).$$

The stabilization parameters for the different methods used in this example are chosen such that the velocity errors in the L^2 norm are minimal. For this we first conduct a series of experiments in which we vary the stabilization parameters of the different methods to study their influence on the solution quality. Our initial triangulation is a four element *criss-cross* mesh. To avoid pre-asymptotic effects, we first refine this mesh five times. Then, we solve the problem for parameters $\delta \in [0.001, 2]$ for the PSPG-stabilization, and $\alpha_i \in [0.01, 20]$, $i = 0, 1$, for the BDG and two-level stabilizations, respectively. By this, we observe that for the PSPG-stabilization, we obtain a good balance of errors at around $\delta_T \approx |T|/12$, which is in line with common recommendations for the practical choice of this parameter. For the projection-based stabilizations we observe optimal errors around $\alpha_i = 1$, which is also justified by linear algebra considerations; cf. [22, Eq. 5.95]. Beyond the optimal choice, all observed error-norms for the PSPG as well as the BDG stabilization begin to increase, which is a clear sign of overstabilization, i.e., unnecessarily strong constraints on the degrees of freedom which would otherwise contribute to a better approximation of the solution. For the proposed two-level-stabilization, the errors do not change significantly for $\alpha_1 > 1$. In fact, the solution is not much different to that obtained by a P_1-iso-$P_2 - P_1$ element for all choices $\alpha_1 \in [1, \infty)$. This kind of (asymptotic) consistency comes from the fact that this stable pairing is recovered in the limit $\alpha_1 \to \infty$ (in exact arithmetics).

Taking the parameters identified by the above experiments, we continue by studying the qualitative characteristics of the different methods based on the benchmark shown above. To quantify the local mass-conservation characteristics, we define

$$|\mathbf{u}_h|_{\operatorname{div},\mathcal{T}_h} := \max_{T\in\mathcal{T}_h} \Big| \int_{\partial T} \mathbf{u}_h \cdot \mathbf{n} \, \mathrm{d}s \Big|, \quad \text{and} \quad |j(\mathbf{u}_h, p_h)|_{\operatorname{div},\mathcal{B}_h} := \max_{B\in\mathcal{B}_h} \Big| \int_{\partial B} j(\mathbf{u}_h, p_h) \, \mathrm{d}s \Big|,$$

where the postprocessed mass flux $j(\mathbf{u}_h, p_h)$ is defined as in the previous section and whenever j is independent of p_h, we shall only write $j(\mathbf{u}_h)$.

We then solve the problem on a series of uniformly refined criss-cross meshes with five consecutive levels using the PSPG stabilization, the BDG stabilization, the two-level stabilized method investigated in this paper, and the classical P_1-iso-$P_2 - P_1$ mixed finite element method. Here we make sure that the resolution of the velocity mesh is the same for all considered cases, i.e., we start with level 2 for the one-level approaches and with level 1 for the two-level approaches. The results are listed in Table 1.

We can observe that all methods perform comparably in the standard norms. Also the observed local mass-defects on the primal mesh do not substantially differ between the different stabilizations. On the dual mesh, however, we see that all considered schemes conserve mass exactly for the post-processed flux (up to roundoff errors). The significance of this property shall be further studied in the following.

TABLE 1

Comparison of different stable $P_1 - P_1$ methods for the colliding flow benchmark on a series of uniformly refined meshes. Rates for the mass-conservative fluxes are omitted since the listed values essentially result from effects of floating point arithmetic, hence contain no meaningful information about the rate of convergence with respect to the mesh-size.

$P_1 - P_1$ element with PSPG-stabilization ($\delta_T = |T|/12$)

$\|\mathbf{u} - \mathbf{u_h}\|_0$	rate	$\|\mathbf{u} - \mathbf{u_h}\|_1$	rate	$\|p - p_h\|_0$	rate	$\|\mathbf{u}_h\|_{\mathrm{div},\mathcal{T}_\mathrm{h}}$	rate	$\|j(\mathbf{u}_h, p_h)\|_{\mathrm{div},\mathcal{B}_\mathrm{h}}$
3.521e+00	-	1.829e+01	-	2.492e+01	-	6.833e-01	-	9.436e-16
9.492e-01	1.89	8.391e+00	1.12	8.716e+00	1.52	1.316e-01	2.38	5.828e-16
2.435e-01	1.96	3.951e+00	1.09	2.756e+00	1.66	1.962e-02	2.75	3.387e-16
6.144e-02	1.99	1.919e+00	1.04	8.315e-01	1.73	2.662e-03	2.88	1.936e-16
1.541e-02	2.00	9.482e-01	1.02	2.470e-01	1.75	3.462e-04	2.94	1.810e-16

$P_1 - P_1$ element with BDG-stabilization ($\alpha_0 = 1$)

$\|\mathbf{u} - \mathbf{u_h}\|_0$	rate	$\|\mathbf{u} - \mathbf{u_h}\|_1$	rate	$\|p - p_h\|_0$	rate	$\|\mathbf{u}_h\|_{\mathrm{div},\mathcal{T}_\mathrm{h}}$	rate	$\|j(\mathbf{u}_h, p_h)\|_{\mathrm{div},\mathcal{B}_\mathrm{h}}$
3.532e+00	-	1.814e+01	-	2.342e+01	-	7.119e-01	-	7.112e-16
9.829e-01	1.85	8.396e+00	1.11	8.476e+00	1.47	1.329e-01	2.42	5.767e-16
2.557e-01	1.94	3.961e+00	1.08	2.758e+00	1.62	1.962e-02	2.76	2.474e-16
6.492e-02	1.98	1.922e+00	1.04	8.538e-01	1.69	2.652e-03	2.89	2.790e-16
1.632e-02	1.99	9.492e-01	1.02	2.593e-01	1.72	3.441e-04	2.95	1.227e-16

$P_1 - P_1$ element with two-level stabilization ($\alpha_1 = 1$)

$\|\mathbf{u} - \mathbf{u_h}\|_0$	rate	$\|\mathbf{u} - \mathbf{u_h}\|_1$	rate	$\|p - p_h\|_0$	rate	$\|\mathbf{u}_h\|_{\mathrm{div},\mathcal{T}_\mathrm{h}}$	rate	$\|j(\mathbf{u}_h)\|_{\mathrm{div},\mathcal{B}_\mathrm{h}}$
3.800e+00	-	1.833e+01	-	2.179e+01	-	8.671e-01	-	8.049e-16
9.082e-01	2.07	8.339e+00	1.14	7.774e+00	1.49	1.336e-01	2.70	8.881e-16
2.249e-01	2.01	3.929e+00	1.09	2.436e+00	1.67	1.910e-02	2.81	3.978e-16
5.605e-02	2.00	1.913e+00	1.04	7.225e-01	1.75	2.554e-03	2.90	4.359e-16
1.399e-02	2.00	9.468e-01	1.01	2.097e-01	1.78	3.301e-04	2.95	2.307e-16

P_1-iso-$P_2 - P_1$ element (stable)

$\|\mathbf{u} - \mathbf{u_h}\|_0$	rate	$\|\mathbf{u} - \mathbf{u_h}\|_1$	rate	$\|p - p_h\|_0$	rate	$\|\mathbf{u}_h\|_{\mathrm{div},\mathcal{T}_\mathrm{h}}$	rate	$\|j(\mathbf{u}_h)\|_{\mathrm{div},\mathcal{B}_\mathrm{h}}$
3.928e+00	-	1.865e+01	-	2.194e+01	-	9.610e-01	-	9.436e-16
9.130e-01	2.11	8.354e+00	1.16	7.741e+00	1.50	1.384e-01	2.80	7.771e-16
2.251e-01	2.02	3.928e+00	1.09	2.409e+00	1.68	1.946e-02	2.83	4.440e-16
5.607e-02	2.01	1.912e+00	1.04	7.088e-01	1.77	2.589e-03	2.91	4.440e-16
1.399e-02	2.00	9.466e-01	1.01	2.034e-01	1.80	3.338e-04	2.96	1.989e-16

5.2. Coupling with advective transport. In this example, we study the effects of mass-conservative flow fields in the context of the coupling of flow and transport. For the sake of simplicity, we are not interested in a fully coupled non-linear simulation here and hence only study the one-way effect of the non-conservative velocity fields on the transport of certain scalar quantities (e.g., concentration, temperature, etc.). We thereby neglect the back-coupling of wrongly convected quantities on the flow field, since this is a highly application-dependent matter and would only complicate the interpretation of our results.

As a model problem, we couple the steady-state Stokes equation (1.1) to a simple transport equation governing the change of mass in a control volume $V_i \subseteq \Omega$, which is given by the integral conservation law

$$\partial_t \int_{V_i} c \,\mathrm{d}\mathbf{x} = -\int_{\partial V_i} c\,\mathbf{u}\cdot\mathbf{n}\,\mathrm{d}s. \tag{5.1}$$

This equates the change of mass in the control volume with the advective transport through the boundary. Let us next assume that Ω is partitioned into non-overlapping polygonal control-volumes V_i. Discretizing spatially in terms of finite volumes (FV) with first-order upwinding (sometimes called donor-cell splitting) and temporally by an forward Euler method on the uniform subdivision $t^k = k\Delta t$, we obtain the explicit marching scheme

$$c_i^{k+1} = c_i^k - \frac{\Delta t}{|V_i|}\sum_{i>j}\left\{(c_i^k + c_j^k)\langle \mathbf{u},\mathbf{n}\rangle_{ij} + (c_i^k - c_j^k)|\langle \mathbf{u},\mathbf{n}\rangle_{ij}|\right\}, \qquad k = 0,1,\ldots,$$

where the degrees of freedom $c_i^k := |V_i|^{-1}\int_{V_i} c(\mathbf{x},t^k)\,\mathrm{d}x$ denote the cell-averages in the control volume V_i at $t = t^k$ and $\langle \mathbf{u},\mathbf{n}\rangle_{ij} := \int_{\partial V_i\cap\partial V_j}\mathbf{u}\cdot\mathbf{n}\,\mathrm{d}s$ denotes the net flux through an interior interface between two control volumes V_i and V_j. Different types of finite volume methods can now be generated by specifying the partitioning of the domain Ω. Below, we shall consider the vertex-centered (VC) scheme with respect to the macro-mesh, i.e., $V_i \in \mathcal{B}_h$ and the cell-centered (CC) scheme with respect to the fine mesh, i.e., $V_i \in \mathcal{T}_h$. The time-step size $\Delta t > 0$ is always chosen small enough, such that the Courant–Friedrichs–Lewy condition is satisfied. For further details on the employed schemes, we refer to [32].

To obtain a non-conservative approximative flow field, we first generate an exact flow field $\mathbf{u}$ as follows: Given the function $\psi_1(\mathbf{x}) := xy(1-x)(1-y)$ and a yet unspecified but smooth enough function $\psi_2(\mathbf{x})$, we set

$$\mathbf{u}(\mathbf{x}) := 10\begin{pmatrix}\partial_y(\psi_1(\mathbf{x})\cdot\psi_2(\mathbf{x}))\\ -\partial_x(\psi_1(\mathbf{x})\cdot\psi_2(\mathbf{x}))\end{pmatrix}, \tag{5.2}$$

which is by construction solenoidal and has free-slip boundary values. This flow field, together with $p(\mathbf{x}) = 10(2x-1)(2y-1)$ is approximately reproduced using the finite element schemes discussed above, where we set boundary conditions given by the exact solution, and we compute $\mathbf{f} = -\Delta\mathbf{u} + \nabla p$ to ensure that $(\mathbf{u},p)$ solves (1.1). The resulting fluxes $\mathbf{u}_h\cdot\mathbf{n}$ and the postprocessed conservative fluxes $j(\mathbf{u}_h,p_h)$ on the boundaries of the control volumes V_i are then used to convect the mass in the discrete sense.

5.2.1. Zeroth order accuracy. In this experiment, we follow the discussion of *zeroth-order accuracy* in [18], i.e., we investigate the capability of the schemes to reproduce a constant initial concentration $c(\mathbf{x},t=0) = 1$ in Ω. In this case, the solution is trivial for an incompressible flow field, since any convected mass is always instantly replaced and thus $c(\mathbf{x},t) = 1$ for all $t \geq 0$. For this, we solve for the interval $t \in (0,1]$. The exact velocity field is generated by plugging the generator function $\psi_2(\mathbf{x}) = (x-\frac{1}{2})^2 + (y-\frac{1}{2})^2$ into the construction given above, producing a complicated flow field with several recirculation zones in the interior of the domain as depicted in Figure 9 (left).

We conduct a series of experiments for a fully unstructured mesh $\mathcal{T}_h$ with the vertex-centered method based on the dual mesh $\mathcal{B}_h$ and the cell-centered method

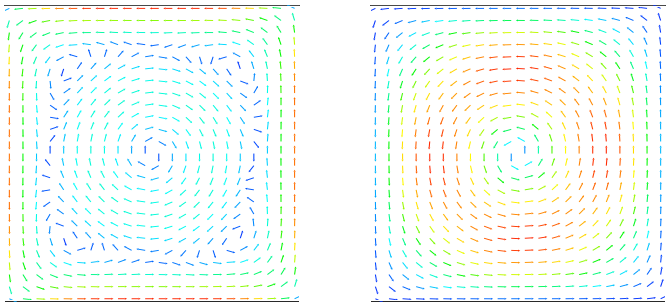

FIG. 9. *Different velocity fields generated by* (5.2) *for different choices of the generator function* ψ_2. *left:* $\psi_2(\mathbf{x}) = (x-0.5)^2 + (y-0.5)^2$*; right:* $\psi_2(\mathbf{x}) = \psi_1(\mathbf{x})/2$. *Arrows are colored by magnitude (red: fast; blue: slow).*

defined on the refinement $\mathcal{T}_{h/2}$. The results for $t = 1$ are depicted in Figures 10 (VC-FV) and 11 (CC-FV). We observe strong mass-defects in the boundary regions, where, the non-conservative fluxes produce errors of $0.5 - 8\%$ for the vertex-centered schemes. These effects grow stronger with increasing stabilization parameters but can be completely avoided by using the newly proposed postprocessing strategies. Using these techniques, the different schemes are all capable of reproducing constant solutions (up to perturbations in the order of numerical roundoff). An interesting observation can be made for the two-level approach: Here we observe significantly smaller mass-defects than for the PSPG or the BDG method already for the method without postprocessing, which indicates the importance of a sufficiently large kernel of the stabilization operator. By considering stabilization terms that have no effect on the macro grid pressures, we achieve better local conservation properties. However, this effect does not carry over to the primal meshes, where for all methods we have to compensate mass-defects of around $7 - 9\%$; see Figure 11.

5.2.2. Mixing of two concentrations. The next example takes a slightly more complicated initial profile which is transported by a single convection cell that can be generated by the choice $\psi_2(\mathbf{x}) = \frac{1}{2}\psi_1(\mathbf{x})$; cf. Figure 9 (right). We set the initial concentration to

$$c(\mathbf{x}, t = 0) = \begin{cases} 2, & x < 0.5, \\ 1, & x \geq 0.5. \end{cases}$$

and solve for the interval $t \in (0, 10]$. The results for $t = 10$ are depicted in Figure 12. We observe that all considered methods display spurious sources and sinks. However, the effect is again less severe for the proposed two-level-stabilized method and can in fact be completely eliminated by postprocessing the velocity solutions. For comparison, we show the results obtained by an over-stabilized PSPG-solution. The over-stabilization of such asymptotically inconsistent (w.r.t. the parameter) stabilizations results in unphysical effects near the boundary which cannot be compensated by the postprocessing alone. The situation is similar for the BDG method. For the two-level-approach the limit yields a stable finite element pair, hence it is not possible to over-stabilize this approach. However, choosing large parameters is not advisable for this approach either, since it has a negative effect on the condition of the resulting linear system of equations.

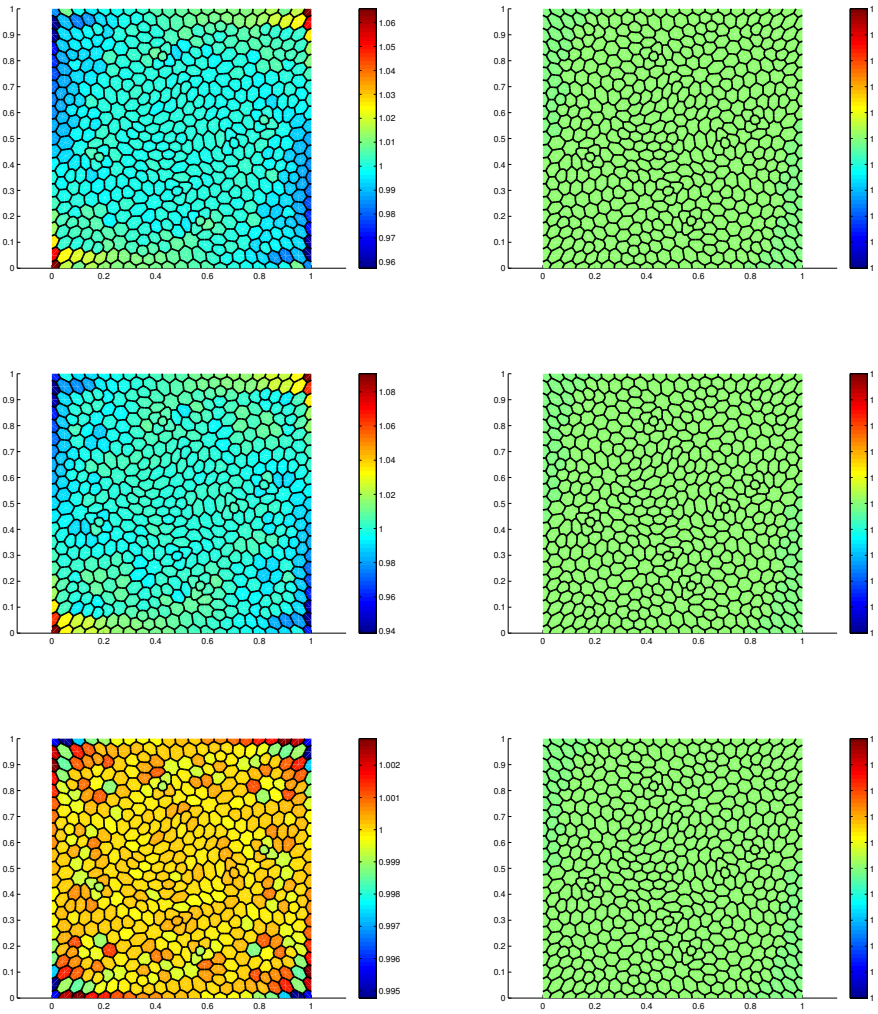

FIG. 10. *Results for $t = 1$ using a VC-FV method: we set the initial concentration to $c(\mathbf{x}, t = 0) = 1$ and compare the velocity fields computed by (from the top row) the PSPG method ($\delta_T = |T|/12$), the BDG method ($\alpha_0 = 1$), the two-level-stabilized method ($\alpha_1 = 1$). On the left, we show the concentration fields obtained without and on the right the ones with postprocessing.*

Acknowledgments. This work was supported (in part) by the German Research Foundation (DFG) through the Priority Programme 1648 "Software for Exascale Computing" (SPPEXA). We would also like to thank the anonymous referees for encouraging us to generalize the theory developed in the course of this work.

REFERENCES

[1] M. Ainsworth and J. T. Oden. *A posteriori error estimation in finite element analysis*. Wiley, Jan. 2000.

[2] D. N. Arnold, F. Brezzi, and M. Fortin. A stable finite element for the Stokes equations.

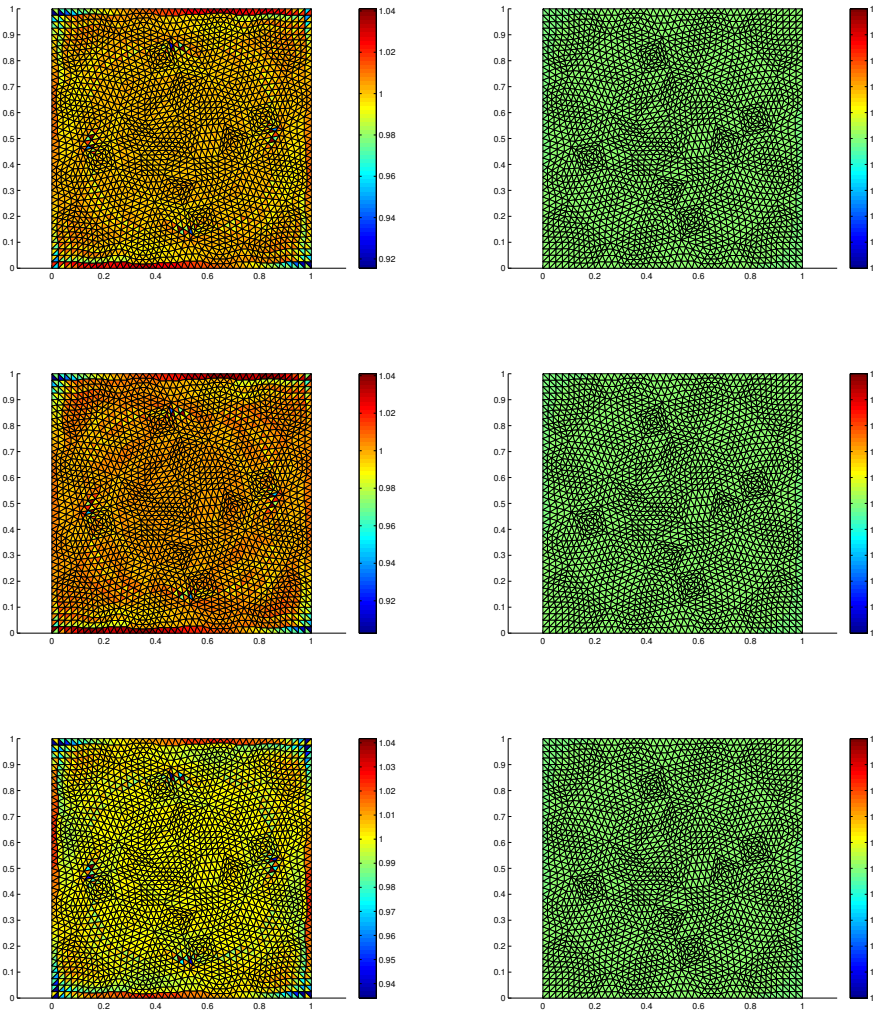

FIG. 11. *Results for $t = 1$ using a CC-FV method: we set the initial concentration to $c(\mathbf{x}, t = 0) = 1$ and compare the velocity fields computed by (from the top row) the PSPG method ($\delta_T = |T|/12$), the BDG method ($\alpha_0 = 1$), the two-level-stabilized method ($\alpha_1 = 1$). On the left, we show the concentration fields obtained without and on the right the ones with postprocessing.*

Calcolo, 21(4):337–344 (1985), 1984.

[3] S. Badia. On stabilized finite element methods based on the Scott–Zhang projector. Circumventing the inf–sup condition for the Stokes problem. *Computer Methods in Applied Mechanics and Engineering*, 247:65–72, 2012.

[4] R. Becker and M. Braack. A finite element pressure gradient stabilization for the Stokes equations based on local projections. *Calcolo*, 38(4):173–199, 2001.

[5] M. Bercovier and O. Pironneau. Error estimates for finite element method solution of the Stokes problem in the primitive variables. *Numerische Mathematik*, 33:211–224, 1979.

[6] P. B. Bochev, C. R. Dohrmann, and M. D. Gunzburger. Stabilization of low-order mixed finite elements for the stokes equations. *SIAM Journal on Numerical Analysis*, 44(1):82–101, 2006.

[7] D. Boffi, F. Brezzi, and M. Fortin. *Mixed finite element methods and applications*. Springer,

2013.

[8] D. Boffi, N. Cavallini, F. Gardini, and L. Gastaldi. Local mass conservation of Stokes finite elements. *Journal of scientific computing*, 52(2):383–400, 2012.

[9] M. Braack and E. Burman. Local projection stabilization for the Oseen problem and its interpretation as a variational multiscale method. *SIAM Journal on Numerical Analysis*, 43(6):pp. 2544–2566, 2006.

[10] F. Brezzi, D. Boffi, L. Demkowicz, R. G. Duran, R. S. Falk, and M. Fortin. *Mixed finite elements, compatibility conditions, and applications*. Springer, Jan. 2008.

[11] F. Brezzi and M. Fortin. *Mixed and hybrid finite element methods*. Springer, New York, New York, 1991.

[12] F. Brezzi and J. Pitkäranta. On the stabilization of finite element approximations of the Stokes equations. In W. Hackbusch, editor, *Efficient Solutions of Elliptic Systems*. Springer, 1984.

[13] M. A. Case, V. J. Ervin, A. Linke, and L. G. Rebholz. A connection between Scott-Vogelius and grad-div stabilized Taylor-Hood FE approximations of the Navier-Stokes equations. *SIAM J. Numer. Anal.*, 49(4):1461–1481, 2011.

[14] S. Chippada, C. Dawson, M. Martinez, and M. Wheeler. A projection method for constructing a mass conservative velocity field. *Computer Methods in Applied Mechanics and Engineering*, 157(1):1–10, 1998.

[15] B. Cockburn, J. Gopalakrishnan, N. C. Nguyen, J. Peraire, and F.-J. Sayas. Analysis of HDG methods for Stokes flow. *Mathematics of Computation*, 80(274):723–760, Apr. 2011.

[16] B. Cockburn, G. Kanschat, D. Schötzau, and C. Schwab. Local discontinuous Galerkin methods for the Stokes system. *SIAM Journal on Numerical Analysis*, 40:319–343, Jan. 2002.

[17] M. Crouzeix and P. A. Raviart. Conforming and Nonconforming Finite Element Methods for Solving to Stationary Stokes Equations I. *Rev. Fr. Automat. Infor.*, 7(3):33–76, 1973.

[18] C. Dawson, S. Sun, and M. F. Wheeler. Compatible algorithms for coupled flow and transport. *Computer Methods in Applied Mechanics and Engineering*, 193(23):2565–2580, 2004.

[19] J.-J. Droux and T. J. R. Hughes. A boundary integral modification of the Galerkin least squares formulation for the Stokes problem. *Computer methods in applied mechanics and engineering*, 113(1):173–182, 1994.

[20] H. Egger and C. Waluga. hp analysis of a hybrid DG method for Stokes flow. *IMA Journal of Numerical Analysis*, 33(2):687–721, 2013.

[21] H. Eichel, L. Tobiska, and H. Xie. Supercloseness and superconvergence of stabilized low-order finite element discretizations of the Stokes problem. *Mathematics of Computation*, 80(274):697–722, 2011.

[22] H. C. Elman, D. J. Silvester, and A. J. Wathern. *Finite Elements and Fast Iterative Solvers: with Applications in Incompressible Fluid Dynamics*. Oxford University Press, New York, 2005.

[23] S. Ganesan, G. Matthies, and L. Tobiska. Local projection stabilization of equal order interpolation applied to the stokes problem. *Mathematics of Computation*, 77(264):2039–2060, 2008.

[24] V. Girault and P. A. Raviart. *Finite Element Approximation of the Navier-Stokes Equations: Theory and Algorithms*. Springer Series in Computational Mathematics. Springer, 1986.

[25] V. Girault, B. Rivière, and M. F. Wheeler. A discontinuous Galerkin method with non-overlapping domain decomposition for the Stokes and Navier-Stokes problems. *Mathematics of Computation*, 74:53–84, 2005.

[26] B. Gmeiner, U. Rüde, H. Stengel, C. Waluga, and B. Wohlmuth. Performance and scalability of hierarchical hybrid multigrid solvers for Stokes systems. Technical report, Chair for System Simulation, University Erlangen-Nuremberg, 2013. submitted.

[27] B. Gmeiner, U. Rüde, H. Stengel, C. Waluga, and B. Wohlmuth. Towards textbook efficiency for parallel multigrid. Technical report, Chair for System Simulation, University Erlangen-Nuremberg, 2013. submitted.

[28] P. Grisvard. *Elliptic problems in nonsmooth domains*. SIAM, Philadelphia, PA, 2011.

[29] A. Hannukainen, R. Stenberg, and M. Vohralík. A unified framework for a posteriori error estimation for the stokes problem. *Numerische Mathematik*, 122(4):725–769, 2012.

[30] F. H. Harlow and J. E. Welch. Numerical calculation of time-dependent viscous incompressible flow of fluid with free surface. *Physics of fluids*, 8:2182, 1965.

[31] T. J. R. Hughes, L. P. Franca, and M. Balestra. A new finite element formulation for computational fluid dynamics: V. circumventing the Babuška-Brezzi condition: a stable Petrov–Galerkin formulation of the Stokes problem accommodating equal-order interpolations. *Computer Methods in Applied Mechanics and Engineering*, 59(1):85–99, 1986.

[32] P. Knabner and L. Angermann. *Numerical methods for elliptic and parabolic partial differential equations*. Springer, 2003.

[33] G. Lube, G. Rapin, and J. Löwe. Local projection stabilization of finite element methods for incompressible flows. In K. Kunisch, G. Of, and O. Steinbach, editors, *Numerical Mathematics and Advanced Applications*, pages 481–488. Springer Berlin Heidelberg, 2008.

[34] R. Luce and B. Wohlmuth. A local a posteriori error estimator based on equilibrated fluxes. *SIAM J. Numer. Anal.*, 42:1394–1414, 2004.

[35] G. Matthies, P. Skrzypacz, and L. Tobiska. A unified convergence analysis for local projection stabilisations applied to the Oseen problem. *ESAIM: Mathematical Modelling and Numerical Analysis*, 41(04):713–742, 2007.

[36] G. Matthies and L. Tobiska. Mass conservation of finite element methods for coupled flow-transport problems. *International Journal of Computing Science and Mathematics*, 1(2):293–307, 2007.

[37] S. Norburn and D. Silvester. Stabilised vs. stable mixed methods for incompressible flow. *Computer Methods in Applied Mechanics and Engineering*, 166(1–2):131 – 141, 1998. Advances in Stabilized Methods in Computational Mechanics.

[38] M. A. Olshanskii and A. Reusken. Grad-div stabilization for Stokes equations. *Mathematics of Computation*, 73(248):pp. 1699–1718, 2004.

[39] O. Pironneau. *Finite element methods for fluids*. Wiley, 1989.

[40] D. Schötzau, C. Schwab, and A. Toselli. Mixed hp-DGFEM for incompressible flows. *SIAM Journal on Numerical Analysis*, 40(6):2171–2194, 2003.

[41] D. Silvester. Optimal low order finite element methods for incompressible flow. *Computer methods in applied mechanics and engineering*, 111(3):357–368, 1994.

[42] L. Song, Y. Hou, and H. Zheng. The two-grid stabilization of equal-order finite elements for the Stokes equations. *International Journal for Numerical Methods in Fluids*, 67(12):2054–2061, 2011.

[43] T. E. Tezduyar, S. Mittal, S. Ray, and R. Shih. Incompressible flow computations with stabilized bilinear and linear equal-order-interpolation velocity-pressure elements. *Computer Methods in Applied Mechanics and Engineering*, 95(2):221–242, 1992.

[44] A. Toselli. hp discontinuous Galerkin approximations for the Stokes problem. *Mathematical Models and Methods in Applied Sciences*, 12(11):1565–1598, 2002.

[45] S. Zhang. A new family of stable mixed finite elements for the 3d Stokes equations. *Mathematics of Computation*, 74(250):543–554, 2005.

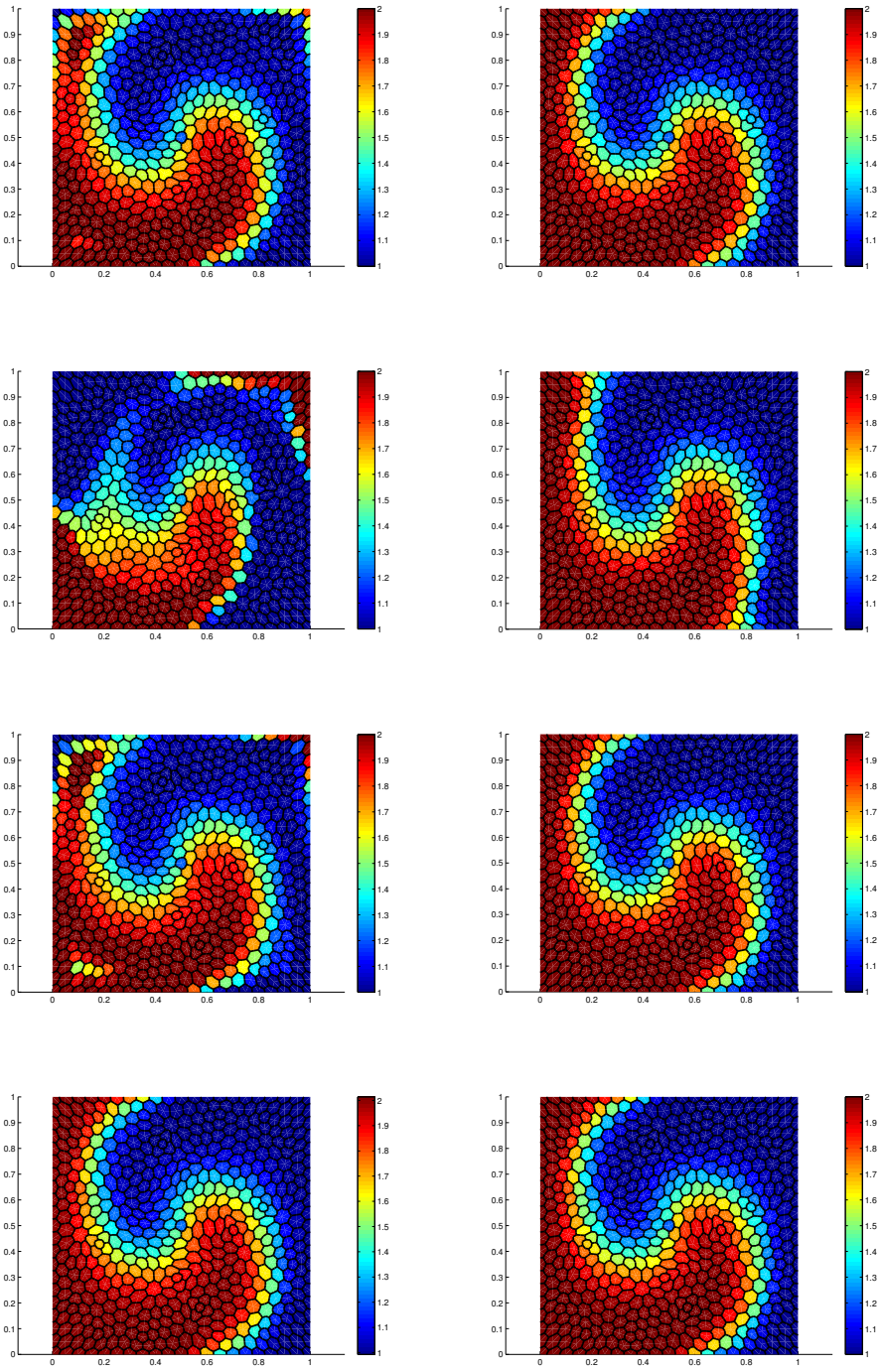

FIG. 12. *Results for $t = 10$ using a VC-FV method: the initial concentration is set to $c(\mathbf{x}, t = 0) = 2$ for $x < 0.5$ and $c(\mathbf{x}, t = 0) = 1$ otherwise. We compare the velocity fields computed by (from the top row) the PSPG method ($\delta_T = |T|/12$), the overstabilized PSPG method ($\delta_T = |T|$), the BDG method ($\alpha_0 = 1$), the two-level-stabilized method ($\alpha_1 = 1$). On the left, we show the concentration fields obtained without and on the right the ones with postprocessing.*